Atmos. Chem. Phys. Discuss., 6, 3513–3570, 2006
www.atmos-chem-phys-discuss.net/6/3513/2006/

Atmospheric Chemistry and Physics Discussions

A modified band approach for the accurate calculation of on-line photolysis rates in stratospheric-tropospheric Chemical Transport Models

J. E. Williams[1], **J. Landgraf**[2], **A. Bregman**[1], **and H. Walter**[2]

[1]Royal Netherlands Meteorological Institute, De Bilt, The Netherlands
[2]SRON National Institute for Space Research, Utrecht, The Netherlands

Received: 16 January 2006 – Accepted: 5 February 2006 – Published: 5 May 2006

Correspondence to: J. E. Williams (williams@knmi.nl)

Abstract

Here we present an efficient and accurate method for the online calculation of photolysis rates relevant to both the stratosphere and troposphere for use in global Chemistry Transport Models. The method is a modified version of the band model introduced by Landgraf and Crutzen (1998) which has been updated to improve the performance of the approach for solar zenith angles >75° without the use of any implicit parameterisations. For this purpose, additional sets of band parameters have been defined for instances where the incident angle of the light beam is between 75–93°, in conjunction with a scaling component for the far UV region of the spectrum (λ=176.6–202.0 nm). For incident angles between 85–93° we introduce a modification for pseudo-sphericity that improves the accuracy of the 2-stream approximation. We show that this modified version of PIFM is accurate for angles <93° by comparing the resulting height resolved actinic fluxes with a recently developed full spherical reference model. We also show that the modified band method is more accurate than the original, with errors generally being ±10% throughout the atmospheric column for a diverse range of chemical species. Moreover, we perform certain sensitivity studies that indicate it is robust and performs well over a wide range of conditions relevant to the atmosphere.

1 Introduction

The incidence of photolysing light on the Earth's atmosphere acts as the principle driving force for many important chemical reaction cycles, which, in turn, play a crucial role towards determining the overall chemical composition of the atmosphere by governing the lifetimes of many key greenhouse species. Many trace gas species exhibit photodissociative rate coefficients (J_x), which can be calculated by integrating the product of the absorption co-efficient (σ_x), the quantum yield (ϕ_x) and the (spectral) actinic flux

ACPD
6, 3513–3570, 2006

($F_{act.}$) over all wavelengths, as described by Eq. (1):

$$J_x = \int \sigma_x(\lambda)\phi_x(\lambda)F_{act}(\lambda)d\lambda \quad (1)$$

Where both σ_x and ϕ_x are characteristic for each specific chemical species (X) and maybe dependent on temperature. The actinic flux ($F_{act.}$) varies with both height and wavelength, and is principally governed by many atmospheric properties, such as the solar geometry, the reflection properties of the Earth's surface, the vertical distribution of ozone, clouds and aerosols and their microphysical properties.

For any model whose aim is to simulate the chemical processes which occur in the atmosphere an important pre-requisite is the inclusion of an accurate code for the calculation of such J rates. Moreover, it is vital that the sphericity of the atmosphere and increased scattering of the incident beam is accounted for during instances of low sun, as this has a direct impact on the magnitude of such rates. Recently, Trentmann et al. (2003) have shown that refraction of light at high solar zenith angles (hereafter referred to as θ) in the upper stratosphere can significantly increase photolysis frequencies by up to 100% in the visible region of the spectrum, which leads to substantial changes in twilight concentrations of many key species. Moreover, using a more complex chemistry-climate model, Lamago et al. (2003) conclude that the depth and extent of ozone destruction simulated for the southern hemisphere is affected by the photolytic production of ClO at the end of the polar winter (where $87.5^{\circ}<\theta<93^{\circ}$). For global 3-D Chemistry Transport Models (CTM's), where the calculation of J values is mandatory, there is also the requirement of computational efficiency, which often requires the use of fast and concise methods in which to calculate J values, thus avoiding excessive runtimes. Therefore, rather than using an infinite number of points which cover the entire spectral range it is necessary to introduce a spectral grid which divides the spectral range into a finite number of bins onto which σ and ϕ values maybe interpolated (e.g. Brühl and Crutzen, 1988; Kylling et al., 1995). However, solving the radiative transfer equation for the each spectral bin individually is still prohibitively expensive, even when using the fastest super-computers, which necessitates the use

of further parameterisations. Thus, values of $F_{act.}$ are commonly calculated offline in many CTM's. These $F_{act.}$ values are usually derived using standard atmospheres under clear-sky conditions, meaning that in many instances, the effect of clouds and aerosols on photolysis rates is not accounted for accurately. Such values are often stored as offline look-up tables which are indexed using atmospheric parameters such as the θ, temperature, pressure, the concentration of overhead O_3 and geo-metric height (e.g. Brasseur et al., 1998; Kouker et al., 1999; Bregman et al., 2000). However, such an approach can be rather inflexible if regular updates are needed to input parameters such as absorption coefficients, where the re-calculation of large look-up tables is often undesirable.

Recently several different methods have been developed which avoid the sole use of look-up tables by performing the online calculation of $F_{act.}$ during each time step in the CTM. Generally, this is made feasible by introducing a much coarser wavelength grid meaning that only a limited number of calculations are needed. For example, Wild et al. (2000) describe the use of an 8-stream RT solver in conjunction with 7 wavelength bins (λ=289–850 nm), in addition to approximations for both single and multiple scattering, for the fast online calculation of J values relevant to the troposphere. This has recently been extended to account for the spectral range relevant to the stratosphere, where a total of 18 wavelength bins are used for the entire spectral range (λ=177–850 nm), with the first 11 being opacity-sorted so as to accurately describe the mean radiation field between 177–291 nm and with Rayleigh scattering being described as a pseudo-absorption (Bian and Prather, 2002). Another example is the recently developed FTUV code, which is based on the TUV radiative transfer model developed by Madronich (1987) and uses a modified wavelength grid between 121–850 nm, where the number of spectral bins is reduced from 140 to 17 (Tie et al., 2004). However, this method is specifically developed for photolysis rates important in the troposphere and therefore was not tuned for species such as N_2O and O_2. The calculation of tropospheric J values is critically dependent on the number of wavelength bins used, where Madronich and Weller (1990) have shown that more than 100 bins are needed

to achieve acceptable errors. Therefore, J values calculated by FTUV still need to have a correction function applied which is dependent on the concentration of overhead O_3, θ and temperature and stored as an offline look-up table.

In this paper we introduce a method for the online calculation of J values relevant to both the troposphere and stratosphere without the use of look-up tables for $F_{act.}$, which can easily be implemented into a state-of-the-art CTM. The method is based on the band approach originally developed by Landgraf and Crutzen (1998), which has been expanded in order to improve the accuracy at high solar zenith angles (hereafter referred to as the modified band approach). For this purpose we have defined additional sets of the band parameters which are used for incident θ>75°, as well as implementing an additional scaling ratio for the far UV region of the spectrum. The explicit nature of this modified approach means that the parameterisation of $J_{abs.}$ as a function of the slant path of the total overhead O_3 and O_2, as described in Landgraf and Crutzen (1998), is no longer needed. This makes the method fully transparent and allows updates/additional photolysis reactions to be added quickly so that the code can potentially fit a host of lumped and explicit chemical reaction schemes.

This paper is arranged as follows: in Sect. 2 we summarise the basic concept of the band approach and outline the modifications introduced for the calculation of J values at high zenith angles. In Sect. 3 we discuss the accuracy of the 2-stream radiative transfer solver used for the calculation of $F_{act.}$ and provide details regarding the pseudo-spherical modification introduced which gives a better account of the effects of spherical geometry for instances of low sun. In Sect. 4 we describe the 1-D column model used to assess the performance of the modified band approach under clear-sky conditions using a range of zenith angles, altitudes and ground albedos. In Sect. 5 we show that the presence of both cloud and aerosol particles makes little difference to the associated errors introduced by the modified band approach. Section 6 provides further discussion regarding the performance for an expanded set of J values and suggestions regarding the implementation of the scheme into other models. Finally, in Sect. 7 we present our concluding remarks.

ACPD
6, 3513–3570, 2006

EGU

2 Description of the method

2.1 The original band approach

In this section we provide a summary of the basic concept behind the modified band approach. In the interests of brevity we simply outline the general approach and for further detail the reader is referred to the more in-depth discussion provided by Landgraf and Crutzen (1998) regarding errors associated with the original method. The spectral grid of Brühl and Crutzen (1988), which covers the spectral range λ=178.6–752.5 nm, is sub-divided into 8 distinct bands and the contributions by each band to each individual photolysis rate is calculated separately (for details of the band limits see Table 1). Calculations are only performed for bands contributing to the photodissociation of a certain species as dictated by the absorption characteristics of that species. Due to the strong absorption by O_2 in the spectral range λ=178.6–202.0 nm, the contribution to $F_{act.}$ by scattering in this spectral range is assumed to be negligible for θ<75°. However, for $\lambda \geq$202 nm, the scattering by gaseous molecules can make a significant contribution to $F_{act.}$ and, therefore, must be accounted for. Moreover, for $\lambda \geq$300 nm the scattering contribution made by both aerosols and clouds must also be accounted for. Landgraf and Crutzen (1998) have shown that the J value for species X maybe approximated by multiplying the $J_{abs.}$ value, calculated in a purely absorbing atmosphere, by a scaling ratio (δ_i) calculated at a specific wavelength (λ_i) within the band limits for band (i) (see Eq. 2):

$$\delta_i = \frac{F_{act}(\lambda_i)}{F_{abs}(\lambda_i)} \quad (2)$$

Where $F_{act.}(\lambda_i)$ is the actual actinic flux at λ_i and $F_{abs.}(\lambda_i)$ the actinic flux for a purely absorbing atmosphere at λ_i. Equation (3) describes $F_{abs}(\lambda)$, which is calculated for each individual wavelength bin assuming the transmission of light adheres to Lambert-Beer's law. Therefore, it is dependent on the slant column depth due to both absorbance by O_3 and O_2 ($\tau_{slant.}(\lambda)$), with $F_0(\lambda)$ being the spectral solar irradiance at the top of the

ACPD
6, 3513–3570, 2006

EGU

atmosphere. The absorption due to both other trace gases (e.g. NO_2), aerosols and clouds is assumed to be negligible compared to that of O_2 and O_3 and is therefore ignored.

$$F_{\text{abs}}(\lambda) = F_0(\lambda)e^{-\tau_{\text{slant}}(\lambda)} \tag{3}$$

Here the slant optical depth ($\tau_{\text{slant.}}(\lambda)$) can be calculated using the density profile ρ_{O2} and ρ_{O3} of oxygen and ozone and their associated absorption cross-sections σ_{O2} and σ_{O3} :

$$\tau_{\text{slant}}(\lambda) = \sum_{x=o3,o2} \int_{o}^{z_{\text{TOA}}} \delta_x \sigma(\lambda)_x dz \tag{4}$$

This resulting $F_{\text{abs}}(\lambda)$ is then used for the calculation of J_{abs}, whose cumulative sum within a band (i) is subsequently scaled by δ_i for the determination of J_i. The scaling ratio (δ_i) need only be calculated for one specific wavelength bin in each of the bands 2–8 and, thus, the full solution of the radiative transfer equation only needs to be performed for a total of 7 distinct wavelength bins. This makes the approach very efficient, as the most computationally expensive step in the derivation of $F_{\text{act.}}$ is the calculation of the scattering component. The J_x value is then calculated by summing all J_i values for species X, as described in Eq. (5), for all bands:

$$J_x = J^{\text{abs.}}_{1,x} + \sum_{i=2}^{8} J^{\text{abs}}_{i,X} . \delta_i \tag{5}$$

The accuracy of the method is principally determined by the extent to which a cancellation of errors occurs within a specific band, where the error per wavelength bin in a band i maybe defined as:

$$\Delta_{i,X}(\lambda) = \left(\frac{F_{\text{act.}}(\lambda)}{F_{\text{act.}}(\lambda_i)} - \frac{F_{\text{abs.}}(\lambda)}{F_{\text{abs.}}(\lambda_i)} \right) \frac{\sigma_X(\lambda)\phi_X(\lambda)}{\sigma_X(\lambda_i)\phi(\lambda_i)} \tag{6}$$

ACPD
6, 3513–3570, 2006

In addition biases in the individual band contribution can cancel out due to the summation in Eq. (5).

2.2 The modified band method

Here we summarise the modifications that have been made to the band method to improve the performance at high zenith angles. The original band limits ($\lambda(i)_{min}$, $\lambda(i)_{max}$) and λ_i as given by Landgraf and Crutzen (1998) for calculating the scaling ratios (δ_i) are summarised in Table 1 and perform well for θ=0–75°. However, due to the increase of the slant optical depth ($\tau_{slant.}(\lambda)$) in instances of low sun, the maximum amount of radiation per band is shifted towards λ of weaker absorption i.e. away from the O_3 absorption maximum. Figure 1 shows the relative actinic flux $\tau(\lambda)=F_{act.}(\lambda)/F_{o.}(\lambda)$ between 300–320 nm normalized to the corresponding value at 310 nm across a range of solar zenith angles. Here the actinic flux below 310 nm decreases relative to the centre wavelength with respect to solar zenith angle, whilst increases occur for wavelengths above 310 nm. In other words, the relative amount of radiation is shifted towards longer wavelengths for larger solar zenith angles due to the longer path length of the direct beam through the atmosphere. This effect holds up until a θ=80°, after which the shift in radiation towards longer wavelengths is weaker. This can be explained by considering the spherical shape of the atmosphere. Until $\theta\approx$80° the path of the solar beam through the ozone layer increases with respect to solar zenith angle until the angle becomes so large that the path length actually begins to decrease due to the spherical shape of the model atmosphere. This effect does not exist when adopting the plane-parallel approximation for the atmosphere. In turn, the band limits and δ_i values of the band model become non-optimal, which subsequently results in errors of between 10–30% which generally occur in the lowest 10km of the atmosphere for important tropospheric species (e.g. J_{H2O2}) when the θ>80°. Moreover, the J values calculated for important stratospheric species such as CFC11 and CH_3Br also exhibit relatively large errors for high solar zenith angles, especially around 30–40 km, where their photolysis is important. In order to reduce the errors the first modification to the method is the

ACPD
6, 3513–3570, 2006

definition of two additional sets of the band limits and λ_i values for instances when the incident θ=75–85° and 85–95°. For an in-depth discussion related to the analysis conducted for determining the choice of these band parameters the reader is referred to Sect. 4.2. These additional sets of band parameters are designated grid A and grid B, respectively, and the details for these grids given in Table 1.

The second modification to the approach is the introduction of a scaling ratio for the first spectral band. An assumption is made in the original band approach that absorption dominates for $\lambda \leq 202$ nm. This assumption only holds for instances when the scattering contribution is negligible compared to the absorption component. As the $\theta > 80°$, the scattering component becomes non-negligible especially for the layers below 60 km due to the longer path length of the direct beam through the upper part of the model atmosphere, which results in a significant source of diffuse light in this altitude range. Therefore, the introduction of a scaling ratio (δ_i) for band 1 for high zenith angles accounts for this. It should be noted that due to assumptions made in the parameterisations of Koppers and Murtagh (1996) and Allen and Frederick (1982) (i.e. a purely absorbing atmosphere) the scaling ratio is not applied during the calculation of either J_{O2} or J_{NO}, respectively. For the lower atmosphere J values are unaffected by the introduction of this scaling ratio due to the effective screening of $\lambda \leq 202$ nm by molecular O_2.

The third modification to the approach is the application of a limit on the scaling ratios (δ_i) for instances where the value of $F_{abs.}$ falls below a selected threshold value. This usually occurs when the slant column increases such that light in the UV spectral region becomes filtered out before it reaches the lower layers. The band approach is sensitive to such events as the resulting scaling ratios (c.f. Eq. 2) may become unrealistically large and result in exaggerated contributions to be made from certain bands to the final J values. Figure 1 shows this effect for band 4 between 300–320 nm, where the scaling ratios become very large due to dramatic decreases of $F_{abs.}$ for high θ. As a consequence the J values in the middle atmosphere (around 30–50 km) may become larger than those calculated higher up the atmosphere for species which exhibit absorbance

ACPD
6, 3513–3570, 2006

EGU

features below λ=320 nm, especially for θ>85°. Moreover, even though the photolysis rates in the troposphere are rather small for instances of very low sun, erroneous increases in the lower 20 km of approximately two orders of magnitude also occur. To solve these problems the scaling ratios (δ_i) adopted for the UV region of the spectrum in the lower layers is set equal to that determined further up the column, where the $F_{abs.}$ is still sufficiently large. Although this modification still introduces an error it is much smaller than that calculated without applying such limits (see Sect. 4.3). In order to negate these artificial increases in rates, a minimum value for $F_{abs.}$ is prescribed for bands 2 to 4, with the respective flux values used for each band being given in Table 2. These limits were applied for all chemical species for instances where θ>85°. Moreover, for species which exhibit strong absorption characteristics for λ<320 nm (e.g. O_3, HNO_3) limits are needed for θ>81°. No limits were applied to bands 1 or 5 through to 8 under any circumstances. For band 1 the scaling ratio only deviates marginally from unity until below 60 km (where the subsequent values never result in an exaggerated band contribution). For the latter bands sufficient light penetrates through to the lower layers for λ>320 nm such that the limits are never reached, even at high zenith angles.

3 Accuracy of the Practical Improved Flux Method

Although many different methods exist for deriving a solution to the radiative transfer equation (e.g. Liou, 2002) we are heavily restricted by the computational burden which radiative transfer schemes introduce. Therefore, to be able to apply this approach in a CTM we have chosen the Practical Improved Flux Method (PIFM), originally derived by Zdunkowski et al. (1980), which uses a 2-stream approximation for calculating the diffuse components of $F_{act.}$. The subsequent error introduced into the final J values as a result of using this 2-stream approximation to calculate $F_{act.}$ values in Eq. (1) has been studied by Landgraf and Crutzen (1998) and is, on average, ~5% for clear-sky conditions and ~20% for cloudy conditions for $\theta \leq 60°$. The maximum errors occur in the middle troposphere where the contributions due to multiple scattering are the greatest.

For higher incident angles ($\theta \geq 80$) the spherical geometry of the atmosphere becomes important which can be a further source of error. For our purposes, we account for this by the use of the air mass correction factor of Karsten and Young (1989) for the calculation of $F_{act.}$ up to $\theta = 85^{\circ}$ (hereafter referred to as PIFM_KY). Comparisons of the resulting height resolved $F_{act.}$ values calculated using PIFM_KY against those calculated using a full spherical reference model (hereafter referred to as reference A) show that the error is only a few percent down to 20 km for $\theta < 85^{\circ}$ across a wide wavelength range (see Appendix A). However, for $\theta \geq 85^{\circ}$ the error increases significantly in the lower atmosphere for heights below 20 km. Therefore, for in such instances we apply a pseudo spherical extension of the PIFM model, where the extinction of the direct beam is described in a spherical manner whereas the diffuse radiative transfer still uses a plane-parallel geometry (hereafter referred to as PIFM_PS). The full details of this modification are comprehensively outlined in Appendix A, where it can be seen that using PIFM_PS only introduces a small error in $F_{act.}$ for zenith angles up to 90°.

The associated errors in the J value profiles for each chemical subset due to the use of the pseudo-spherical solver at high incident angles are discussed in Appendix B of this paper. In general the errors are in the order of ±2% except in the lowest layers. Here the error increases significantly to ±30% in some instances. However, these errors are always related to extremely small values of $F_{act.}$, and thus, are of minor importance for the estimate of photolysis rates in a CTM. In general, these errors for $\theta > 85^{\circ}$ are much smaller than those introduced by the modified band method (see Sect. 4.5 and Fig. 9).

4 Development of the low sun band settings

4.1 Description of the 1-D column model

The testing and subsequent tuning of the modified band approach was performed using a standard 1-D column model. The vertical grid consisted of 80 equidistant layers

ACPD
6, 3513–3570, 2006

of 1 km depth from the ground level to the top of the atmosphere. The pressure, temperature, relative humidity and O_3 concentrations were taken directly from the U.S. standard atmosphere (NOAA, 1976) and interpolated onto the vertical grid. The total ozone column is scaled to 300 DU to allow direct comparisons with the results presented in Landgraf and Crutzen (1998). For brevity we limit the discussion below to comparisons made between a version of the model which uses PIFM to calculate $F_{act.}$ explicitly for each wavelength bin without the use of a look-up table for the temperature dependent σ and ϕ values (hereafter referred to as reference B) versus the final working version of the photolysis scheme as implemented into the stratosphere-troposphere version of TM5 (manuscript in preparation). This comparison determines the error introduced solely by the band method. The final working version was the result of several upgrades to the original code driven by the need to remove the most computationally expensive steps. The slant column for each layer/level combination is calculated in a similar manner to that documented by Madronich (1987) and is imperative for the correct $F_{abs.}$ values in the lowest layers (and thus scaling ratios). In Appendix A we have shown that, when applying a modification for the effects of spherical geometry, PIFM-PS is capable of calculating values of $F_{act.}$ within an acceptable error limit across a range of incident θ values up to 90°. It should be noted that any error due to PIFM-PS is additional to the errors introduced by the band method.

In the stratospheric-tropospheric version of TM5 photodissociation rates are calculated for a total of 38 separate chemical species, which have been identified as being important for studying the impact of chemical processes that occur across the diverse range of chemical regimes present in the troposphere and stratosphere. Table 3 provides an overview of the individual photolysis reactions calculated online, along with details related to the absorption coefficients (σ_x) and quantum yields (ϕ_x) used for the determination of the J values. All σ_x and ϕ_x values were chosen according to the latest recommendations (e.g. Sander et al., 2003; Atkinson et al., 2004) and subsequently interpolated onto the spectral grid of Brühl and Crutzen (1988), where 142 spectral bins are used between 178.6–752.5 nm (of varying resolution). For molecular O_2 the

absorption in the Lyman-Alpha and Schumann-Runge regions of the spectrum are accounted for using the parameterizations of Chabrillat and Kockarts (1997) and Koppers and Murtagh (1996), respectively. For the photolysis of NO, which occurs in the far UV, the parameterization of Allen and Frederick (1982) is implemented. Temperature dependencies of σ values are included for 17 of the chosen chemical species (see Table 3). Moreover, a temperature dependency for the ϕ related to O^1D production from the photolysis of O_3 was also included as recommended by Matsumi et al. (2002). In order to remove expensive interpolation steps, a look-up table of these temperature dependent quantities was produced using a resolution of 5°C over the temperature range 180–340°C and indexed using the temperature of each atmospheric layer. Various look-up tables with differing resolutions between 1–10°C were tested and the 5°C resolution found to be both accurate and concise. For the calculation of the Rayleigh scattering cross-sections the empirical approach of Nicolet (1984) is used. Details concerning the treatment of aerosol particles and cloud layers are given in Sect. 5. For all calculations the ground was treated as a Lambertian reflector using albedo values ranging between 0–100%, with the value of the albedo being fixed across the entire spectral range.

For the purpose of assessing the associated errors, and to avoid an exhaustive analysis involving all 38 photolysis reactions, we define two smaller subsets of the species with each subset being photolytically relevant to either the stratosphere or the troposphere (see Table 4). One of the conditions involved in the selection of these two chemical subsets was that the absorption behavior was sufficiently diverse enough to be able to test the modified band method across the entire spectral range. The number of photolysis rates added for stratospheric species has been significantly increased compared to the original treatise of Landgraf and Crutzen (1998) meaning that the performance of the both the original and modified band method is being tested for such compounds for the first time (e.g. BrO).

ACPD
6, 3513–3570, 2006

4.2 Selection of the band limits

One of the requirements of the photolysis scheme presented here is the accurate calculation of height resolved J values for a diverse range of species over the entire atmospheric column. This introduces certain limitations regarding the modifications which can be made to the spectral range over which such J values are calculated, even for instances of low sun. This is due to the percentage contribution by each band to each J value being dependent on height for many chemical species. Figure 2 shows the variation in the percentage contributions by each spectral band designated in the band method for two layers for J_{O3} and J_{BrNO3} with respect to the zenith angle under clear sky conditions. These contributions are derived using the original band settings as given in Table 1. Here it can be seen that J_{O3} is principally determined by contributions originating from band 3, which contains the absorption maximum for O_3. In contrast, due to the overhead O_3 column being relatively low at this altitude and the broad absorption characteristics of $BrNO_3$, contributions are made to J_{BrNO3} across the entire spectral range i.e. bands 1 to 8. Moreover, the contribution made by each band to J_{BrNO3} only changes marginally as the zenith angle increases until $\theta \approx 90^{\circ}$. However, nearer the ground the percentage contributions change considerably as a consequence of the effective screening of the far UV by molecular O_2 and O_3. This removes all contributions made by bands 1 to 3 in the lower layers, resulting in a decrease in the J values with respect to height (e.g. Figs. 3a/c). As the value of J_{O3} in the lower layers decreases with increasing angle (not shown), the percentage contribution made by band 4 also decreases (with an associated increase in the percentage contribution made by band 6) until $\theta = 80^{\circ}$. For $\theta > 80^{\circ}$ the contribution by band 4 increases again due to the sphericity of the Earth's atmosphere. At these geometries the path length of the direct beam through the ozone layer decreases with an increasing solar zenith angle. In turn, the relative amount of radiation is shifted towards shorter wavelengths, which increases the contribution from band 4. The features shown for bands 5 and 6 can also be explained by this effect. For J_{BrNO3} a similar effect is observed near ground level, where

the contributions from bands 1 to 3 are screened out meaning that J_{BrNO3} is principally determined by the contributions from bands 7 and 8. Therefore, truncating the spectral grid at either end of the spectral range for high zenith angles is not possible without introducing large associated errors in either the stratosphere or troposphere.

For the determination of the band parameters for θ>75° various combinations of $\lambda(i)_{min}$, $\lambda(i)$ and $\lambda(i)_{max}$ were tested and the resulting errors in the J values assessed to discern whether any significant reduction in errors occurred compared to the original band settings. A limitation was found to exist in the choice of band limits for band 4 due to many of the species in the tropospheric subset exhibiting strong absorption in the spectral range covered by this band. Therefore, the resulting errors for such species were very sensitive to where the limits for this band were placed on the spectral grid. For bands 5 to 8 it was found that the accuracy of the method was increased by shifting the band limits and $\lambda(i)$ towards the visible end of the spectrum, although $\lambda(8)_{max}$ remained unchanged. This procedure was performed for the zenith angle ranges θ=75–85° and θ=85–95°, resulting in parameter grids A and B, respectively (see Table 1). These grids were used for the calculation of all J values listed in Table 3, with the exceptions of J_{O2} and J_{NO}, for the specified ranges of θ.

4.3 The variation in the associated errors for θ=72–85°

In this section we investigate the performance of the modified band approach under clear sky conditions using grid A and compare the resulting errors with those calculated using the original band settings.

Figures 3a–d show the typical variation in J values, with respect to height, for both the stratospheric and tropospheric chemical subsets under clear sky conditions at θ=80° and assuming an albedo of 5%. These profiles were calculated using the operational version of the photolysis scheme in conjunction with the original band settings. The saw-tooth feature, which is evident in the error diagrams for certain species, is due to the use of the look-up table for the temperature dependent σ values (c.f. the smooth error profiles which exist for species that have no temperature dependencies). The cor-

responding errors when using grid A for both chemical subsets are shown in Figs. 4a and b. By comparing Figs. 3b/d with Figs. 4a/b it can be seen that the application of grid A leads to substantially lower errors compared to reference model B, especially for J_{BrO}, J_{CFC12}, J_{COH2}, and J_{H2O2}, where the error is approximately halved. It should be noted that the increase in the associated error for both J_{N2O} and J_{CFC12} below 40 km relates to J values that are very small which tends to amplify the error introduced by small differences.

Figures 5a–d and 6a–h show the variation in the error associated with the J values calculated using the original band settings for the stratospheric and tropospheric chemical subsets, respectively, over the range θ=72–85°. The corresponding contour plots of the associated error calculated using grid A, as well as a scaling ratio for band 1 and limits for δ_i in the lower layers, are given in Figs. 7a–d and 8a–h, respectively.

By comparing these figures it can be seen that there are substantial reductions in the associated errors obtained using the modified version of the band approach for both of the chemical subsets. For the stratospheric subset only a small selection of the species are shown, with the other species in each subset having associated errors of ±3% for both the original and modified version of the approach (although a reduction in error is always observed using the new band parameters). For the species shown all associated errors are below 10% for the first 50 km of the column across the entire range of θ, with the exception of J_{CFC12}. Here, the error drops substantially in the middle atmosphere due the use of the scaling ratio for band 1 (the band limits are identical for band1 between the original grid and grid A – see Table 1). It is also interesting to note that for the original band settings as the incident zenith angle increases some chemical species exhibit a reduction in the associated error as the contributions by each band to the total J value change (e.g. J_{BrO}, Fig. 5c).

For the tropospheric subset the associated errors are larger for the bottom 25 km of the column, especially for the original band settings. The zenith angle at which the associated errors show a significant increase is θ=82°, with the exception of J_{NO2} (Fig. 6b). This is due to an over-estimation of the band contribution made by band 4

ACPD
6, 3513–3570, 2006

EGU

to the final J value when using the original method, as a consequence of a large δ_i value (i.e. low $F_{abs.}$, see Sect. 2.2). The dramatic reduction in the associated errors due to the application of limits on the δ_i value is clear when comparing Figs. 6a and 8a. Although some error is still introduced by applying such limits (between ±10–20% for the lowest 10 km, see Fig. 8a) the magnitude of the maximum error drops by an order of magnitude. Similar improvements are seen for an additional six species from the tropospheric subset, although limits are only applied for O_3, HNO_3 and HNO_4. Application of the limits across all species results in a decrease in the accuracy of the modified band method for species such as H_2O_2 due to the characteristic absorption properties exhibited within particular bands (not shown). Therefore, for $\theta \leq 85^\circ$, the use of such limits should be tested for each particular species included within the photolysis scheme. The species for which it is applied in TM5 are indicated in the comprehensive list of photolysis reactions given in Table 3.

The sensitivity of the band method to the values of σ and ϕ can be elucidated by comparing Fig. 4a with Fig. 5 in Landgraf and Crutzen (1998). Here, the associated errors calculated for J_{O3} ($\rightarrow O^1D$) are approximately double those shown in the original investigation using the original band settings when no limits are applied to the scaling ratio. This arises from updating the method in which ϕ is determined (where the temperature dependent σ values originate from Molina and Molina (1986) in both cases). The original quantum yield was taken from the study of Talukdar et al. (1998), whereas the one adopted here was based on the recommendation of Matsumi et al. (2002), which is a critical synthesis of many independent studies. This update leads to substantial differences especially in the contribution made by the fourth band to J_{O3} and, more importantly, the contribution to the total J value made by each wavelength bin (not shown). From this it maybe concluded that the errors associated with the band method are critically dependent on the input parameters used to determine the individual photolysis rates. Therefore, it should be noted that any future updates may affect the absolute values of the associated errors presented here.

Finally, as a means of testing the sensitivity of the band method to the variation in the

total overhead O_3 column (i.e. optical depth) duplicate calculations were performed using various scaling factors of between 250–400 DU (not shown). No significant change in the distribution of the associated errors compared to those shown for 300 DU were observed, indicating that the performance of the band method is relatively robust over a range of atmospheric conditions.

4.4 The effect of ground albedo on the associated errors

For brevity we limit the investigation of the impact of ground albedo to those photolysis rates which are most important near the ground as this is where the largest perturbation occurs. Also not shown are the results calculated using the original band settings but simply those calculated using grid A. Figures 9a and b show the influence of ground albedo on the associated error for J_{O3} and J_{HNO3}, respectively, at θ=80° using grid A. For all instances the surface is assumed to behave as a Lambertian Reflector i.e. a homogeneous surface. From these figures it can be seen that the performance of the modified band approach is fairly robust across the entire range of ground albedos, and, in general, the errors remain rather constant for both of the chemical species shown. All the other species in the tropospheric subset exhibit associated errors in the ±2% range. Therefore, it can be concluded that the modified band approach can be used with confidence over a diverse range of reflecting surfaces.

4.5 The variation in the associated errors for θ=85–93°

For zenith angles >85°, the magnitude of the $F_{act.}$ values in the middle and lower layers of the atmosphere (below 50 km) are essentially governed by the diffuse radiation i.e. the $F_{abs.}$ contribution becomes very small (see Fig. 1). As with zenith angles <85°, this has unwanted numerical consequences resulting in large values for the δ_i ratios calculated for bands 1 through to 4 which results in unrealistically large J values. Therefore, the limit for the scaling ratios was applied to the first four bands between θ=85–93°. For the tropospheric subset of species, the values for $F_{act.}$ become so small

near the surface that the resulting J values become rather unimportant when considering the diurnally integrated rates (see Fig. A3, Appendix A). However, we did ensure that the J value profiles for such species do not exhibit spurious increases near the ground. Thus, we limit the following discussion to the errors associated with the stratospheric subset of chemical species calculated when using grid B, in conjunction with the PIFM-PS solver.

Figures 10a–d show the associated errors calculated for J values over the range θ=85–90° for a select number of species from the stratospheric chemical subset thought to be the most important for polar chemical ozone depletion at such high incident angles (Lamago et al., 2003). The errors are generally below 20% with the exception of J_{ClNO3} (Fig. 10c). Unsurprisingly, when compared to the associated errors for θ=72–85°, many of the associated errors for this θ range are approximately an order of magnitude larger, even though the band parameters are further updated to those defined in grid B (see corresponding plots show in Fig. 7). This is partly due to the application of the limits to the scaling ratios across the entire range for λ=176–320 nm i.e. the J values become moderately smaller then those calculated using reference B. However, grid B still leads to a substantial reduction in the associated errors compared to J values calculated with both the original grid and grid A (not shown).

Although it is possible to calculate J values with PIFM-PS up to an incident zenith angle of 95° (see Appendix A), the small values of both F_{act} and F_{abs} result in large errors being introduced at angles above θ=93° for similar reasons to those discussed above. Moreover, many of the J values become so small under such conditions that the computational expense of performing the calculation is often not warranted. Therefore, the analysis presented here only includes results between θ=90–93°, calculated for 0.5° intervals. Figures 11a–d show the associated errors for J values over the incident range θ=90–93° for the corresponding species shown in Fig. 10. It can be seen that for these species an error of ±5% occurs above 35 km, which is considered to be very good. Larger errors occur between 20–30 km for θ>91.5°, as would be expected due to the decrease in the magnitude of the direct beam. The blue diagonal error contour

in Figs. 11a–c (for errors >5%) essentially indicates the height at which the incident light begins to diminish (see Fig. A3 in Appendix A). It should be noted that although the errors increase substantially below 30 km, the respective J values are so small that even a +100% error does not perturb the chemical system in any appreciable manner.

5 The effect of clouds and aerosols

Here we investigate the effect of aerosol particles and clouds on the error associated with the J values calculated using the modified band approach. Again, for brevity we only present the results calculated using grid A. In global CTMs clear-sky conditions almost never exist due to the ubiquitous presence of aerosols, liquid water clouds and ice water clouds (with the cloud fraction, liquid water content and ice water content usually being defined by the meteorological input data). The effect of both clouds and aerosol on atmospheric processes via the perturbation of the radiation field has been extensively discussed in the literature (e.g. He and Carmichael, 1999; Haywood and Boucher, 2000; Tie et al., 2004). For the aerosols in this study we prescribe particles throughout the entire column and select "rural" aerosol for the lower 4 km and "background" aerosol for the rest of the column, using optical properties taken from Shettle and Fenn (1979) and particle number densities as defined by McClatchey et al. (1972). The difference between these aerosol types is that the "background" aerosol has a smaller absorption component compared to the "rural" type in conjunction with a lower particle number density. The particle number density of each layer was scaled such that the integrated optical depth due to the aerosol column was 0.32 at 550 nm, in line with the settings chosen in Landgraf and Crutzen (1998).

The contribution to both absorption and scattering introduced by cloud layers was calculated using the parameterization of Slingo (1989). The cloud fraction is taken into account in the radiative transfer calculations of F_{act} using the approach of Geleyn and Hollingsworth (1979). For our purpose, two cloud layers were introduced with 100% cloud coverage at 1–2 km and 7–8 km with optical densities of 24.9 and 38.3,

respectively. Moreover, we assume a fixed radius of 8 μm for the cloud droplets. To account for aerosols within the cloud the relative humidity (*RH*) of any atmospheric layer containing a cloud fraction >95% is assumed to be between 98–99% (i.e.) near saturation. The absorption and scattering properties of the aerosol increase with *RH* and the corresponding aerosol optical depth increased to 0.52 at 550 nm due to the increase in *RH* in the cloud layers.

5.1 The effect of aerosol on the J value errors

Figure 12 shows the effect of aerosol particles in the 1-D column model on the *J* value profiles calculated for the tropospheric subset at θ=80°. For this purpose comparisons are made against *J* value profiles calculated under clear sky conditions using the modified band approach, therefore differentiating the effect of aerosol. This figure shows that the largest reduction occurs in the bottom 15 km of the atmosphere, where the concentration of aerosol particles is the highest. Above this height the effect on the *J* values is of the order of 1–2% (i.e. there is a negligible effect on the stratospheric chemical subset – not shown). This is particularly true for higher incident angles due to the increased absorption component in the lower 4 km (i.e. the "rural" aerosol) and the increased scattering introduced into the overhead atmospheric column as a consequence of the increase in the slant path. These effects cause differences of ~–7% and ~–2–20%, respectively, with the largest difference being exhibited for J_{NO2} (blue solid line in Fig. 12). This behaviour is somewhat different to the original results shown in Landgraf and Crutzen (1998), where calculations were performed using the DISORT method for θ=0° and an albedo =0%. Identical calculations for θ=80° using DISORT revealed that similar reductions as those shown in Fig. 10 occur.

The associated errors for the tropospheric subset with respect to the incident angle are very similar to those shown in Fig. 8 when compared to reference B, and therefore, are not shown or subsequently discussed. For the "urban" aerosol, as defined by Shettle and Fenn (1979), which exhibits a higher absorption component than the "rural" aerosol, there is a larger reduction in the *J* values for the bottom layers compared

ACPD
6, 3513–3570, 2006

to Fig. 12. Moreover, the effect extends further up the column (to ∼30 km) as a consequence of a reduction in the upwelling flux (not shown). In summary, although the magnitude of the J values are affected in the bottom 20 km of the column, the overall accuracy of the modified band approach remains unaffected by the increase in optical depth introduced by a typical aerosol column using a variety of aerosol types.

5.2 The effect of cloud and aerosol on the J value errors

The final analysis presented in this paper focuses on the combined effect of both cloud and aerosol on the performance of the modified band approach. For details concerning the distribution of optical density though the column the reader is referred to the introductory text in Sect. 5. Such conditions pertain to the type of scenarios commonly encountered in a typical CTM. For the tropospheric species the effect on the J values is similar to that shown in Fig. 7 of Landgraf and Crutzen (1998) and therefore is not reproduced here, although the effects are more marked as a consequence of the higher zenith angles. The effects above 40 km are minimal due to the cloud being situated much lower down the atmospheric column. Generally there is an enhancement in J values for the stratospheric subset of between 2–12%, with those species exhibiting absorption in the visible region being affected the most.

For the variation of the associated errors with respect to the incident angle there is little change for the stratospheric species, with the magnitude of the errors being very similar to those shown for clear sky conditions (see Fig. 7). The associated errors for the tropospheric species, as shown in Figs. 13a–d, reveals that there is a re-distribution and, in some instances, a change in the associated error for a few of the species shown in Fig. 8. However, the associated errors for the species shown in Fig. 13 are generally still within ±10% in the lower 10 km, even though the optical density of the column increases. Moreover, it should be noted that this result pertains to a worst-case scenario of 100% cloud coverage. In a CTM the majority of grid cells have smaller cloud fractions and thus, smaller changes in the associated errors compared to the clear-sky scenario. In summary, no significant degradation in the accuracy of the band method

occurs for cloudy conditions.

6 Further discussion

6.1 Other chemical species

For the J values calculated for the additional chemical species listed in Table 2 there are corresponding improvements in the accuracy of the modified band method using both grids A and B compared to the original default settings. The remaining species may, again, be sub-divided into those species which are photolytically important for either the troposphere or the stratosphere.

For the zenith angle range θ=72–85° the additional stratospheric species generally exhibit a reduction in the associated error above 30 km using grid A for clear-sky conditions compared with the original method (namely $J_{CH3ONO2}$, J_{CFC11}, J_{CFC113}, J_{CH3Cl}, J_{CH3Br}, J_{HOCl} and J_{HOBr}). Below this height there is an increase in the associated error for most of these J values, although in many instances the J values are unimportant at these altitudes. For the additional tropospheric species, again, a reduction in the associated error is observed for J_{CH4CO}, $J_{CH3COCHO}$, $J_{CH3COCH3}$, $J_{CH3COOH}$, J_{PAN} and both channels of J_{NO3}. The most dramatic reductions in error occur for those species which exhibit large contributions from band 4 (e.g. CH_3COCH_3). Another notable example is the photolysis of NO_3 which falls to ±3% in the lowest 10 km compared to −5–10% obtained using the original band settings. The only exception to this trend is a small increase in error for $J_{O3}p$ (reaching ∼8% compared with ∼3% for the lowest few layers of the atmosphere).

For scenarios which include cloud and aerosols, there are similarities in the change in the distribution of the associated errors as discussed in Sect. 5.2. Associated errors of between 5–10% exist from 0–25 km for all the additional tropospheric species except J_{CH4CO} , which has similar band contribution as for J_{O3d} and thus exhibits an increase in the lowest layer at θ=82°. For the additional stratospheric species there is only a

ACPD
6, 3513–3570, 2006

EGU

minimal effect on the associated errors compared to the clear-sky scenario discussed above.

6.2 The feasibility of future updates

The photolysis scheme presented here has been specifically designed to calculate height resolved J values for chemical species which are photolytically important to the chemical composition of both the tropospheric and stratospheric, in line with the first application in the stratospheric-tropospheric version of TM5. Therefore, if one wished to use such a scheme for a model which focuses purely on the troposphere, where the photolysis of species such as, for example, the CFC's and N_2O are not important, then modifications could be made to the approach (e.g. the removal of band 1). It should be noted that for any additional species the associated error depends on which bands contribute to the final J value. Chemical species with absorption maxima at λ>305.5 nm will have rather small associated errors, such as e.g. dimethyl sulfide (DMS). Moreover, new values for the photolytic parameters (σ_x and ϕ_x) can be easily implemented into the scheme due to the transparent nature in which the scheme has been designed (i.e.) by simply updating the look-up table by interpolating the updated values onto the working grid.

7 Conclusions

In this paper we have presented a flexible, efficient and accurate scheme for the online calculation of height resolved photolysis rates for zenith angles in the range 75–93°, which has been designed specifically for the implementation into global Chemistry Transport Models. For this purpose, we have extended the band method of Landgraf and Crutzen (1998) for θ>75°. The result is an enhanced performance in instances of low sun for a diverse range of chemical species. For θ>85° we have made use of a pseudo-spherical extension of a two-stream radiative transfer solver, PIFM

ACPD
6, 3513–3570, 2006

(Zdunkowski et al., 1980). This results in a significant reduction in the errors as compared against a full spherical reference model. The errors on the resulting J values are generally of the order of ±2% for regions of the atmosphere important at these very high zenith angles.

For the band method we have introduced modifications which significantly improve the accuracy of the approach, these being: (i) the definition of two additional sets of band parameters (for θ=72–85° and θ=85–90°, respectively), (ii) a scaling ratio for the far UV which accounts for the reduced direct flux for θ>75° in the middle atmosphere and (iii) a threshold for the calculation of scaling ratios below 320 nm. In general, the errors introduced by the modified band method are in the region of ±10% or lower over the range θ=72–85° for species relevant to both the troposphere and the stratosphere. This dramatically improves the performance of the modified band method especially for species such as O_3 and HNO_3 for θ>80°. Moreover, the threshold for the scaling ratios is also applied to bands 1 through to 4 for θ>85°, which results in associated errors to be of the order of −10% between 30–80 km for many important stratospheric species over the range θ=85–90°. For θ>90° the associated errors are typically between ±5% above 40 km, although as the scenario moves towards a purely scattering atmosphere the errors increase markedly for the lower layers due to the assumptions made by the band method. However, many J values become so small in the bottom layers for high zenith angles that this increase in error does not have important consequences.

Finally, we have tested the performance of the modified band method in the presence of both cloud and aerosols, and over a wide range of ground albedo's and total overhead O_3 column densities, and subsequently shown that the method is both robust and accurate over a range of conditions typically found in the atmosphere.

Appendix A

The pseudo spherical two-stream model

The generalized two-stream approximation of scalar radiative transfer in its plane parallel geometry may be expressed by (Liou, 2002):

$$\frac{1}{\beta_{\text{ext}}}\frac{dF^+}{dz} = \alpha_1 F^+ - \alpha_2 F^- - \alpha_3 I_o \quad \text{(A1)}$$

$$\frac{1}{\beta_{\text{ext}}}\frac{dF^-}{dz} = \alpha_2 F^+ - \alpha_1 F^- + \alpha_4 I_o \quad \text{(A2)}$$

$$\frac{\mu_o}{\beta_{\text{ext}}}\frac{dI_o}{dz} = I_o \quad \text{(A3)}$$

where F^+ and F^- are the upward and downward fluxes and I_o describes the solar radiances, z represents the altitude, β_{ext} is the extinction coefficient, and the coefficients α_1 to α_4 are given by :

$$\alpha_1 = U(1 - \omega(1 - \beta_o)) \quad \text{(A4)}$$

$$\alpha_2 = U\beta_o\omega \quad \text{(A5)}$$

$$\alpha_3 = \omega\beta(\mu_o) \quad \text{(A6)}$$

$$\alpha_4 = (1 - \omega)\beta(\mu_o). \quad \text{(A7)}$$

Here U is the diffusivity factor, ω is the single scattering albedo, β_o is the fractional mean backward scattering coefficient and $\beta(\mu_o)$ is the backward scattering coefficient of the direct solar beam, where μ_o is the cosine of the solar zenith angle (θ). The values for the diffusivity factor and the backscattering coefficients depend on the particular

two-stream approximation. In this paper we make use of the Practical Improved Flux Method (PIFM) (Zdunkowski et al., 1980) utilizing the following parameters:

$$U = 2 \tag{A8}$$

$$\beta_o = \frac{3 - p_1}{8} \tag{A9}$$

$$\beta(\mu_o) = \frac{1}{2} - \frac{\mu_o}{4} p_1 \tag{A10}$$

where p_1 is first coefficient of an expansion of the scattering phase function in terms of Legendre polynomials.

Equations (A1–A3) can be solved by using standard methods for a vertically inhomogeneous atmosphere which is sub-divided into a number of homogenous layers. Using the solution for F^+, F^- and I_o, the actinic flux can be approximated by:

$$F_{\text{act}} = U(F^+ + F^-) + I_o. \tag{A11}$$

To take into account effects of the Earth sphericity on the radiative transfer one can use, as a first correction to the plane parallel approach, the air mass of a spherical model atmosphere for the attenuation of the direct beam. Therefore we modify the air mass factor (μ_o^{-1}) in Eq. (A3) by a corresponding expression suggested by Kasten and Young (1989);

$$f(\gamma) = \frac{1}{\sin\gamma + a(\gamma + b)^{-c}} \tag{A12}$$

Where γ is the solar elevation angle and values for the empirical constants of a=0.5057, b=6.08°, and c=1.636.

A more sophisticated method of representing sphericity is the pseudo-spherical approximation (e.g. Walter et al., 2004). Here the Lambert-Beers absorption law of the direct beam in Eq. (A3) is replaced by a corresponding equation for spherical geometry:

$$\frac{1}{\beta_{\text{ext}}} \frac{dI_o}{ds} = I_o \tag{A13}$$

with s being the path length of the direct beam through a spherical atmosphere with respect to the global zenith angle, as indicated in Fig. A1. Solving this equation, the direct light can be coupled into the flux equation of a plane parallel atmosphere via Eqs. (A1) and (A2). Therefore, one has to bear in mind that for θ>90° the solar beam does not illuminate the upper boundary of a particular atmospheric layer anymore but its lower boundary. In turn we have to modify the coefficients α_3 and α_4 accordingly:

$$\alpha_3 = [\Theta(\mu_o)\varpi + \Theta(-\mu_o)(1-\varpi)]\beta(\mu_o) \quad \text{(A14)}$$

$$\alpha_4 = [\Theta(-\mu_o)(1-\varpi) + \Theta(\mu_o)\varpi]\beta(\mu_o) \quad \text{(A15)}$$

where Θ is the Heavy-Side step function. These modified flux equations can subsequently be solved using the method described by Zdunkowski et al. (1980).

To give an estimate regarding the accuracy of both the Kasten and Young correction and the pseudo-spherical extension of the PIFM model, we have compared simulations of the actinic flux with those calculated using a reference model. The reference model is based on a finite element method, which solves the radiative transfer equation for a spherical shell medium. Therein, the singly scattered contribution of the radiation field is calculated analytically, whereas the multiply scattered contribution can be computed via a two-dimensional Picard iteration. Both components of the radiation field are calculated taking the spherical geometry of the radiative transfer problem into account. Further details related to the reference model may be found in Walter et al. (2006)[1] and Doicu et al. (2005).

Figures A2a and b show the percentage differences in F_{act} obtained when comparing the plane parallel PIFM model, the PIFM model using the modified air mass factor of Kasten and Young (1989), and the pseudo-spherical extension of the PIFM model with the spherical reference model (this work) at λ=326.5 nm and λ=610 nm, respectively. For θ<70°, the different versions of PIFM provide almost identical results for the chosen altitude levels, where differences compared with the reference model never exceed

[1]Walter, H. H., Landgraf, J., Spada, F., and Doicu, A.: Linearization of a radiative transfer model in spherical geometry, J. Geophys. Res., submitted, 2006.

5%. However, at θ>80° the simple plane-parallel model clearly deviates from the modified versions of PIFM, with the largest errors occurring at the lower altitudes (c.f. 60 km with 20 km). Similar effects occur for θ>85° using the Kasten and Young air mass correction factor. In contrast, the pseudo spherical PIFM model provides very accurate estimates of the actinic flux up to θ=90°. It should be noted that the pseudo spherical model is much more computationally expensive than the Kasten and Young approximation meaning that it's application is only warranted when the increase in accuracy is significant (i.e.) above 85°.

Figures A3 and A4 show the accuracy of the pseudo spherical PIFM model for θ=91–95°. At 326.5 nm the actinic flux decreases significantly between 25–70 km altitude due to the attenuation of the direct beam by Rayleigh scattering and ozone absorption (see Fig. A3). Here the actinic flux starts to decrease already at higher altitudes for higher incident angles, due to the longer path of the direct light through the atmosphere. At 610.0 nm the direct beam is much less attenuated, which results in a less marked decrease in the F_{act} with respect to altitude (see Fig. 4). For this wavelength the F_{act} decreases to very small values in the shadow of the Earth body, where only the diffuse component of the radiation is present. The pseudo spherical version of PIFM can reproduce this feature very well and overall the corresponding errors are small. Only at altitudes where the contribution of the direct beam to F_{act} is negligible because of either the strong extinction which exists in the photon path or due to the shadow of the Earth body, the error increases to up to 30%. However, due to the small values of F_{act} at these altitudes this large error is of minor importance for our application.

ACPD
6, 3513–3570, 2006

Appendix B

The associated error in the subset J values due to the pseudo-spherical PIFM model

Although the error in $F_{act.}$ calculated using the PIFM-PS solver is of the order of a few percent at various heights throughout the atmosphere up to θ=90° (see Appendix A), the subsequent error with respect to the final J values for both the tropospheric and stratospheric chemical subsets also needs to be quantified. Due the high computational effort involved in using the full spherical reference model the calculation of J value profiles using full spherical geometry was not possible within a reasonable time. Therefore, for the purpose of quantifying the error in the J values we have interpolated the height resolved $F_{act.}$ values calculated for the scaling wavelengths chosen for grid A (see Table 1) onto the working grid of Brühl and Crutzen (1988) for all 80 atmospheric layers. The subsequent error for each wavelength bin (in terms of photons $nm^{-1} s^{-1}$) was then calculated by taking the difference between the $F_{act.}$ values resulting from the reference model A and PIFM-PS. By scaling this difference using the characteristic σ and ϕ values for each chemical species, we are able to quantify the corresponding errors in the J value profiles at any particular zenith angle. Figures B1a and b show the associated errors due to PIFM-PS at θ=90° for both the stratospheric and tropospheric subsets, respectively. These figures show that the errors for the first 40 km of the column are generally of the order of ±2%. Below this height the error increases substantially for species such as N_2O, although the actual J value at this altitude is extremely small. For the other tropospheric species the errors down to 25 km are below ±5%, after which negative errors exist for all species. Fortuitously, the J values become rather irrelevant at such high zenith angles in the lower portion of the column meaning that the effect on the overall performance of the PIFM_PS is minimal.

Figure B2 shows the corresponding errors for the worst case scenario of θ=93° (see Sect. 4.5). Again, the associated errors in the J values for the top 40 km due

to PIFM-PS were ±2%, except for J_{N2O}. Below this height there is so little direct flux below 320 nm which penetrates through to the lower levels that the $F_{act.}$ for this spectral region is determined almost purely by scattering. Therefore, the contributions by bands 1 to 4 subsequently decrease, resulting in lower errors in the J values for the lowest 20 km of the column compared to θ=90°. In summary, the modification to the 2-stream approximation outlined in Appendix A reduces the error introduced by using the 2-stream approximation significantly, especially at the altitudes important during instances of very low sun (θ>90°).

Acknowledgements. J. E. Williams acknowledges financial support from the European Commision Sixth Framework program SCOUT-O3 (505390-GOCE-CT-2004). A. Bregman acknowledges financial support from the National User Support Programme run by the Netherlands User Support Programme (GO2(EO-066)).

References

Allen, M. and Frederick, J. E.: Effective photodissociation cross sections for molecular oxygen and nitric oxide in the Schumann–Runge bands, J. Atmos. Sci. , 39, 2066–2075, 1982.

Atkinson, R., Baulch, D. L., Cox, R. A., Hampson Jr., R. F., Kerr, J. A., Rossi, M. J., and Troe, J.: Evaluated kinetic and photochemical data for atmospheric chemistry, Supplement V, IUPAC Subcommittee in Gas Kinetic Data Evaluation, J. Phys. Chem. Ref. Data., 26(3), 521–1011, 1997.

Atkinson, R., Baulch, D. L., Cox, R. A., Crowley, J. N., Hampson Jr., R. F., Hynes, R. G., Jenkin, M. E., Kerr, J. A., Rossi, M. J., and Troe, J.: Summary of evaluated kinetic and photochemical data for atmospheric chemistry, IUPAC Subcommittee in Gas Kinetic Data Evaluation, Web Version, http://www.iupac-kinetic.ch.cam.ac.uk, 2004.

Bian, H. and Prather, M. J.: Fast-J2: Accurate simulations of Stratospheric Photolysis in Global Chemical Models, J. Atmos. Chem., 41, 281–296, 2002.

Brasseur, G. P., Hauglustaine, D. A., Walters, S., Rasch, P. J., Muller, J.-F., Granier, C., and Tie, X.: MOZART, a global chemical tracer model for ozone and related chemical tracers. 1. Model description, J. Geophys. Res., 103, 28 265–28 289, 1998.

Bregman, A., Lelieveld, J., van den Broek, M. M. P., Siegmund, P. C., Fischer, H., and Bujok, O.: N_2O and O_3 relationship in the lowermost stratosphere: a diagnostic for mixing processes as represented by a three-dimensional chemistry-transport model, J. Geophys. Res., 105, 17 279–17 290, 2000.

Brühl, C. and Crutzen, P. J.: Scenarios of possible changes in atmospheric temperatures and ozone concentrations due to man's activities, estimated with a one-dimensional coupled photochemical climate model, Clim. Dyn., 2, 173–203, 1988.

Chabrillart, S. and Kockarts, G.: Simple parameterization of the absorption of the solar Lyman-Alpha line, Geophys. Res. Lett., 24(21), 2659–2662, 1997, also: Correction: Geophys. Res. Lett., 25(1), 79, 1998.

Doicu, A., Trautmann, T., Schreier, F., and Hess, M.: Finite element method for the two-dimensional atmospheric radiative transfer, J. Quant. Spect. Radiat. Trans., 91, 347–361, 2005.

Geleyn, J. F. and Hollingsworth, A.: An Economical analytical method for the computation of the interaction between scattering and line absorption of radiation, Contrib. Atmos. Phys., 52(1), 1–16, 1979.

Haywood, J. and Boucher, O.: Estimates of the direct and indirect radiative forcing due to tropospheric aerosols: a review, Rev. Geophys., 38, 513–543, 2000.

He, S. and Carmicheal, G. R.: Sensitivity of photolysis rates and ozone production in the troposphere to aerosol properties, J. Geophys. Res., 104, 26 307–26 324, 1999.

Karsten, F. and Young, A. T.: Revised optical air mass tables and approximation formula, Appl. Opt., 28, 4735–4738, 1989.

Koch, S. and Moortgat, G. K.: Photochemistry of Methylglyoxal in the vapour phase, J. Phys. Chem. A, 102, 9142–9153, 1998.

Koppers, G. A. A. and Murtagh, D. P.: Model studies of the influence of O_2 photodissociation parameterizations in the Schumann-Runge bands on ozone related photolysis in the upper atmosphere, Ann. Geophys., 14, 68–79, 1996.

Kouker, W., Langbein, I., Reddmann, T., and Runke, R.: The Karlsruhe Simulation Model of the Middle Atmosphere (KASIMA), Version 2, Forsch. Karlsruhe, Wiss Ber No. 6278, Karlsruhe, Germany, 1999.

Kylling, A., Stamnes, K., and Tsay, S.-C.: A reliable and efficient two-stream algorithm for spherical radiative transfer: Documentation of accuracy in realistic layered media, J. Atmos. Chem., 21, 115–150, 1995.

Lamago, D., Dameris, M., Schnadt, C., Eyring, V., and Brühl, C.: Impact of large solar zenith angles on lower stratospheric dynamical and chemical processes in a coupled chemisty-climate model, Atmos. Chem. Phys., 3, 1981–1990, 2003.
Landgraf, J. and Crutzen, P. J.: An Efficient Method for online calculations of Photolysis and Heating Rates, J. Atmos. Sci., 55, 863–878, 1998.
Lenoble, J.: Atmospheric Radiative Transfer, Deepak, p. 532, 1993.
Liou, K. N.: An Introduction to Atmospheric Radiation, Academic Press, p. 31, 2002.
Madronich, S.: Photodissociation in the atmosphere: 1, Actinic Flux and the effect of ground reflections and clouds, J. Geophys. Res., 92, 9740–9752, 1987.
Madronich, S. and Weller, G.: Numerical integration errors in calculated tropospheric photodissociation rate co-efficients, J. Atmos. Chem., 10, 289–300, 1990.
Matsumi, Y., Comes, F. J., Hancock, G., Hofzumahus, A., Hynes, A. J., Kawasaki, M., and Ravishankara, A. R.: Quantum yields for production of $O(^1D)$ in the ultraviolet photolysis of ozone: Recommendation based on evaluation of laboratory data, J. Geophys. Res., 107(D3), 4024, doi:10.1029/2001JD000510, 2002.
McClatchey, R. A., Fenn, R. W., Selby, J. E. A., Volz, F. E., and Garing, J. S.: Optical properties of the atmosphere, Environ. Res. Paper., 411, AFCRL-72-0497, pp. 108, 1972.
Molina, L. T. and Molina, M. J.: Absolute absorption cross sections of ozone in the 185 to 350 nm wavelength range, J. Geophys. Res., 91, 14 501–14 508, 1986.
Nicolet, M.: On the molecular scattering in the terrestrial atmosphere: an empirical formula for it's calculation in the homosphere, Planet. Space. Sci., 32, 1467–1468, 1984.
NOAA: US Standard Atmosphere, 1976 National Oceanic and Atmospheric Administration NOAA-S/T76-1562, Washington D.C., U.S. Govt Printing office, 227, 1976.
Sander, S. P., Friedl, R. R., Ravishankara, A. R., Golden, D. M., Kolb, C. E., Kurylo, M. J., Huie, R. E., Orkin, V. L., Molina, M. J., Moortgart, G. K., and Finlayson-Pitts, B. J.: Chemical Kinetics and Photochemical Data for Use in Atmospheric studies, Evaluation No. 14, JPL Publication 02-25, 2003.
Shettle, E. P. and Fenn, R. W.: Models for the aerosols of the lower atmosphere and the effects of the humidity variations on their optical properties, Environ. Res. Paper, 676, AFGL-TR-79-0114, 91 pp., 1979.
Slingo, A.: A GCM parameterization for the shortwave radiative properties of water clouds, J. Atmos. Sci., 46, 1419–1427, 1989.
Schemansky, D. E.: CO_2 Extinction Co-efficient 1700–3000 Å, J. Chem. Phys., 56, 1582–1587,

1972.
Talukdar, R. K., Longfellow, C. A., Gilles, M. K., and Ravishankara, A. R.: Quantum yields of O(1D) in the photolysis of ozone between 289 and 329 nm as a function of temperature, Geophys. Res. Lett., 25, 143–146, 1998.
Tie, X., Madronich, S., Walters, S., Zhang, R., Rasch, P., and Collins, W.: Effect of clouds on photolysis and oxidants in the troposphere, J. Geophys. Res., 108, 4642, doi:10.1029/2003JD003659, 2003.
Trentmann, J., Bovensmann, H., Eyring, V., Muller, R. W., and Burrows, J. P.: Impact of Accurate Photolysis Calculations on the simulation of Stratospheric chemistry, J. Atmos. Chem., 44, 225–240, 2003.
Walter, H. H., Landgraf, J., and Hasekamp, O.: Linearization of a pseudo-spherical vector radiaitive transfer model, J. Quant. Spectr. Radiat. Trans., 85, 251–283, 2004.
Wild, O., Zhu, X., and Prather, M. J.: Fast-J: Accurate simulation of in- and below-cloud photolysis in global chemical models, J. Atmos. Chem., 43, 245–282, 2000.
Zdunkowski, W. G., Welsch, R. M., and Korb, G. J.: An investigation of the structure of typical 2-stream methods for the calculation of solar fluxes and heating rates in clouds, Contrib. Atmos. Phys., 53, 215–238, 1980.

Table 1. Wavelengths chosen for the lower and upper band limits, and for the derivation of scaling ratios (δ_i) in the operational version of the modified band approach. Values for θ<75° are taken from Landgraf and Crutzen (1998) and those for θ=75–85° (A) and θ=85–95° (B) as derived in this study.

Band	λ_{min}	λ_{max}	λ_{scale}	λ_{min}(A)	λ_{max}(A)	λ_{scale}(A)	λ_{min}(B)	λ_{max}(B)	λ_{scale}(B)
1	178.6	202.0	N/A	178.6	202.0	199.0	178.6	202.0	201.0
2	202.0	241.0	205.1	202.0	243.9	209.4	202.0	243.9	213.9
3	241.0	289.8	287.7	243.9	289.8	287.7	243.9	289.8	287.7
4	289.8	305.5	302.0	289.8	305.5	302.0	289.8	305.5	302.0
5	305.5	313.5	309.0	305.5	313.5	311.0	305.5	312.5	311.0
6	313.5	337.5	320.0	313.5	347.5	326.5	312.5	357.5	345.0
7	337.5	422.5	370.0	347.5	482.5	385.0	357.5	492.5	410.0
8	422.5	752.5	580.0	482.5	752.5	610.0	492.5	752.5	610.0

Table 2. Thresholds for F_{abs} used in the calculation of the scaling ratios for bands 2 to 4 at high zenith angles. The unit for F_{abs} is photons $nm^{-1}\ s^{-1}$.

Band	θ: 82–85°	θ: >85°
2	1×10^{9}	1×10^{9}
3	–	1000.
4	2×10^{9}	2×10^{8}

ACPD
6, 3513–3570, 2006

Table 3. Details concerning the literature values adopted for the characteristic absorption co-efficients and quantum yields for all photolytically active chemical species included in the global CTM TM5, where (*) denotes temperature dependent parameters. A value of unity is assumed for the quantum yields of species where there is a lack of laboratory data. Reactions given in red are those for which limits are applied to the δ ratios above θ=81°. For θ>85° limits are applied to all photolysis rates to avoid problems in the middle atmosphere (see Sect. 2.2).

Photolysis reaction	Absorption co-efficient	Quantum yield
$O_2 \xrightarrow{h\nu} O^{3P}+O^{3P}$	Chabrilla and Kockarts (1994) (λ=121–123 nm) Koppers and Murtagh (1996) (λ=nm) Sander et al. (2003) (λ>178.6 nm)	1.0
$O_3 \xrightarrow{h\nu} O_2+O^{1D}$	Molina and Molina (1986)*	Matsumi et al. (2002)*
$O_3 \xrightarrow{h\nu} O_2+O^{3P}$	Molina and Molina (1986)*	Matsumi et al. (2002)*
$NO_2 \xrightarrow{h\nu} NO+O^{3P}$	Sander et al. (2003)*	Sander et al. (2003)
$NO_3 \xrightarrow{h\nu} NO+O_2$	Sander et al. (2003)	Sander et al. (2003)
$NO_3 \xrightarrow{h\nu} NO_2+O^{3P}$	Sander et al. (2003)	Sander et al. (2003)
$N_2O \xrightarrow{h\nu} N_2+O^{1D}$	Sander et al. (2003)*	1.0
$N_2O_5 \xrightarrow{h\nu} NO_2+NO_3$	Sander et al. (2003)	1.0
$H_2O_2 \xrightarrow{h\nu} 2OH$	Sander et al. (2003)*	1.0
$HNO_3 \xrightarrow{h\nu} OH+NO_2$	Sander et al. (2003)*	1.0
$HNO_4 \xrightarrow{h\nu} HO_2+NO_2$	Sander et al. (2003)	1.0
$CH_2O \xrightarrow{h\nu} HCO+H$	Sander et al. (2003)*	Sander et al. (2003)
$CH_2O \xrightarrow{h\nu} CO+H_2$	Sander et al. (2003)*	Sander et al. (2003)
$CH_3CHO \xrightarrow{h\nu} CH_4+CO$	Martinez et al. (1992)	Atkinson et al. (2004)
$CH_3COCHO \xrightarrow{h\nu} CH_3CO_3+CO+HO_2$	Atkinson et al. (1997)	Koch and Moortgat (1998)
$CH_3COCH_3 \xrightarrow{h\nu} CH_3CO_3+CH_3O_2$	Atkinson et al. (1997)	McKeen et al. (1997)
$CH_3OOH \xrightarrow{h\nu} CH_3O+OH$	Sander et al. (2003)	1.0

Table 3. Continued.

Photolysis reaction	Absorption co-efficient	Quantum yield
$CH_3O_2NO_2 \xrightarrow{h\nu} CH_3O_2 + NO_2$	Atkinson et al. (1997)	1.0
$PAN \xrightarrow{h\nu}$ Products	Sander et al. (2003)*	1.0
$OClO \xrightarrow{h\nu} ClO + O^{3P}$	Sander et al. (2003)	1.0
$ClNO_3 \xrightarrow{h\nu} Cl + NO_3$	Sander et al. (2003)*	Atkinson et al. (2004)
$CH_3Cl \xrightarrow{h\nu}$ Products	Sander et al. (2003)*	1.0
$CCl4 \xrightarrow{h\nu}$ Products	Sander et al. (2003)*	1.0
$CF_2ClCFCl_2 \xrightarrow{h\nu}$ Products	Sander et al. (2003)	1.0
$CCl_3F \xrightarrow{h\nu}$ Products	Sander et al. (2003)*	1.0
$CCl_2F_2 \xrightarrow{h\nu}$ Products	Sander et al. (2003)	1.0
$BrNO_3 \xrightarrow{h\nu} Br + NO_3$	Sander et al. (2003)	1.0
$CH_3Br \xrightarrow{h\nu}$ Products	Sander et al. (2003)*	1.0
$BrCl \xrightarrow{h\nu} Br + Cl$	Sander et al. (2003)*	1.0
$HCl \xrightarrow{h\nu} H + Cl$	Sander et al. (2003)	1.0
$HOCl \xrightarrow{h\nu} OH + Cl$	Sander et al. (2003)	1.0
$HOBr \xrightarrow{h\nu} OH + Br$	Sander et al. (2003)	1.0
$BrO \xrightarrow{h\nu} Br + O^{3P}$	Sander et al. (2003)*	1.0
$Cl_2O_2 \xrightarrow{h\nu} Cl + ClO_2$	Sander et al. (2003)	1.0
$H_2O \xrightarrow{h\nu} H + OH$	Sander et al. (2003)	1.0
$CO_2 \xrightarrow{h\nu} CO + O^{3P}$	Schemansky (1972)	1.0
$NO \xrightarrow{h\nu} N + O^{3P}$	Allen and Frederick (1982)	1.0

ACPD
6, 3513–3570, 2006

EGU

Table 4. Details of the two chemical subsets selected for the derivation of the low sun band settings and for the quantification of the performance of the modified band approach. The spectral range indicates the spectral region over which each species exhibits absorption.

Troposphere		Stratosphere	
Photolysis reaction	Spectral range [nm]	Photolysis reaction	Spectral range [nm]
$O_3 \xrightarrow{h\nu} O_2 + O^{1D}$	219.8–342.5	$N_2O \xrightarrow{h\nu} N_2 + O^{1D}$	178.6–241.0
$NO_2 \xrightarrow{h\nu} NO + O^{3P}$	202.0–422.5	$OClO \xrightarrow{h\nu} ClO + O^{3P}$	259.7–477.5
$N_2O_5 \xrightarrow{h\nu} NO_2 + NO_3$	178.6–382.5	$Cl_2O_2 \xrightarrow{h\nu} Cl + ClO_2$	178.6–452.5
$HNO_3 \xrightarrow{h\nu} OH + NO_2$	178.6–352.5	$ClNO_3 \xrightarrow{h\nu} Cl + NO_3$	196.1–362.5
$HNO_4 \xrightarrow{h\nu} HO_2 + NO_2$	178.6–327.9	$BrNO_3 \xrightarrow{h\nu} Br + NO_3$	178.6–497.5
$H_2O_2 \xrightarrow{h\nu} 2OH$	178.6–347.5	$BrO \xrightarrow{h\nu} Br + O^{3P}$	311.5–392.5
$CH_2O \xrightarrow{h\nu} HCO + H$	298.1–347.5	$CCl_2F_2 \xrightarrow{h\nu} Products$	178.6–241.0
$CH_2O \xrightarrow{h\nu} CO + H_2$	298.1–357.5	$BrCl \xrightarrow{h\nu} Br + Cl$	200.0–602.5

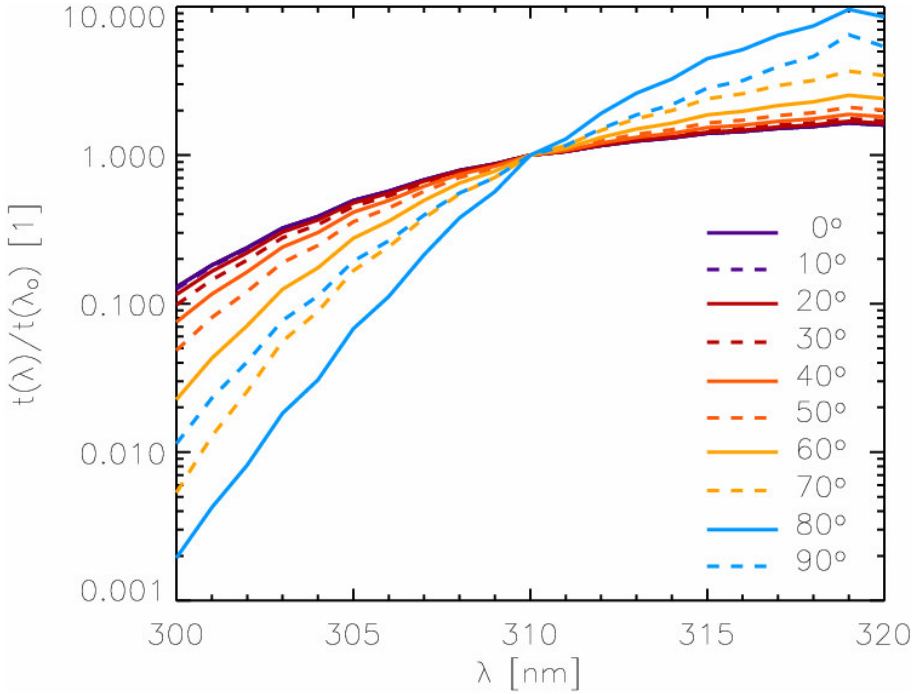

Fig. 1. Relative actinic flux $\tau(\lambda)=F_{act.}(\lambda)/F_{o.}(\lambda)$ between 300–320 nm normalized to the corresponding value at 310 nm as a function of solar zenith angle. For details regarding the 1-D column model used the reader is referred to Sect. 4.1. Calculations were performed using the original band settings in conjunction with the original input parameters for the temperature dependent σ and ϕ of O_3. The total ozone column was scaled to 300 DU and the ground albedo =5%.

ACPD
6, 3513–3570, 2006

EGU

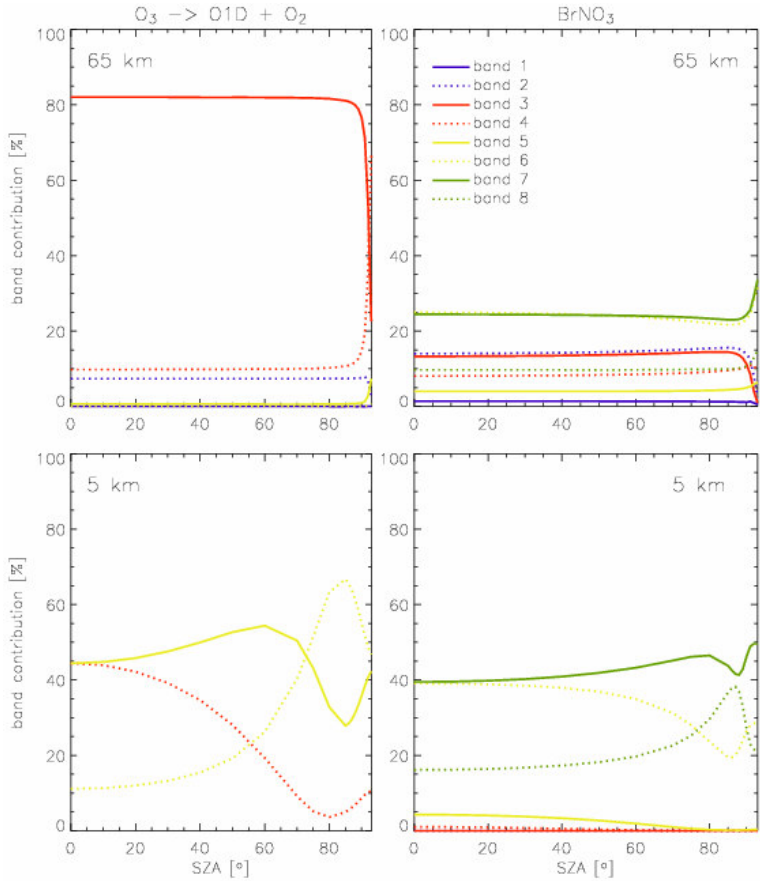

Fig. 2. The percentage contributions made by each spectral band for the calculation of $J_{O3}\rightarrow O^1D$ and J_{BrNO3} at 5 and 65 km using the band method. These contributions were determined using the original band settings taken from Landgraf and Crutzen (1998). The total ozone column was scaled to 300 DU and a ground albedo =5%.

ACPD
6, 3513–3570, 2006

EGU

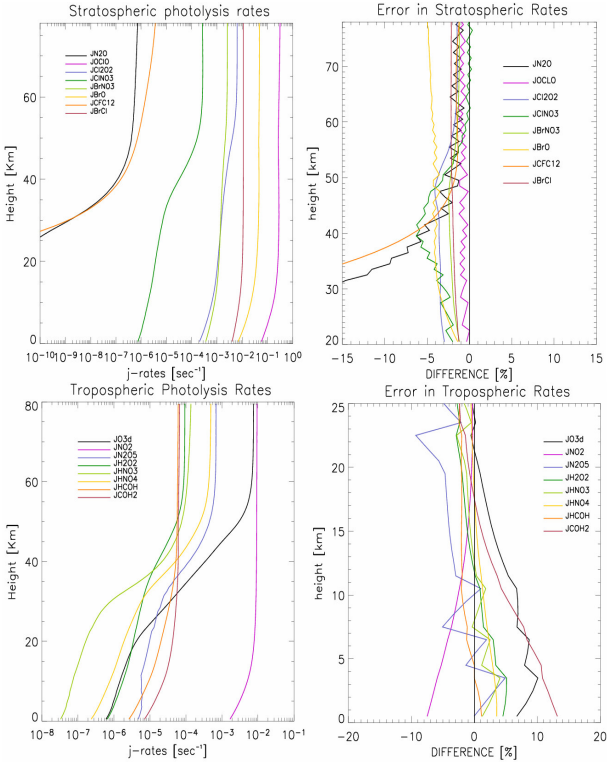

Fig. 3. (a) Typical J value profiles for the stratospheric subset of species at θ=80° and a ground albedo =5% with **(b)** associated errors introduced by using the band approach with the original band settings as taken from Landgraf and Crutzen (1998) in conjunction with a 5°C resolution look-up table as compared with a reference model (see text). Panels **(c)** and **(d)** show the corresponding information for the tropospheric subset.

ACPD
6, 3513–3570, 2006

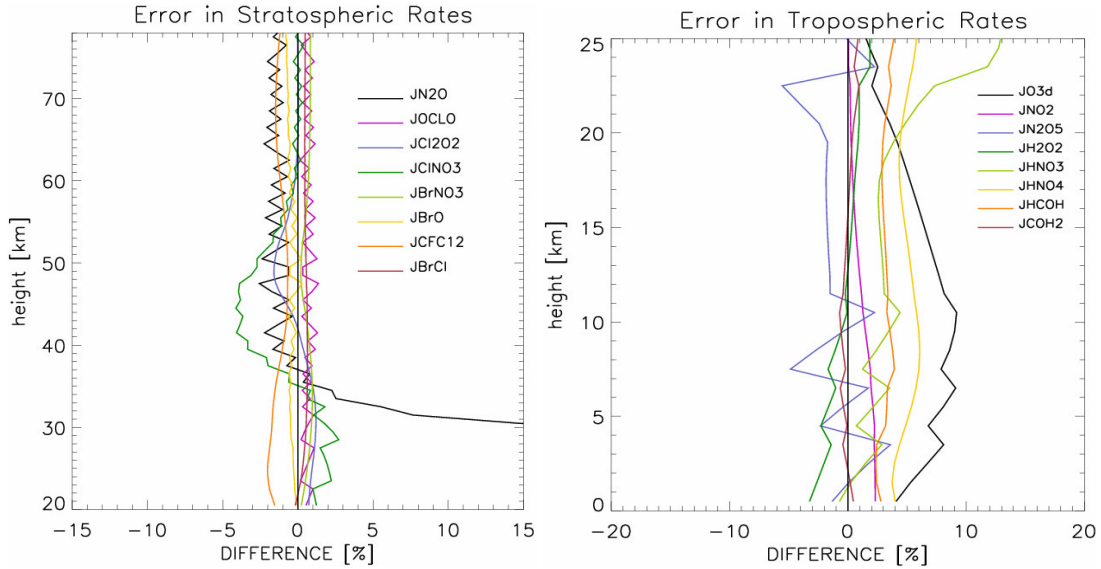

Fig. 4. Corresponding errors in the J value profiles using the modified band approach in conjunction with grid A for θ=80° with an albedo of 5%. An identical atmosphere is used as for Figs. 3a/b.

ACPD
6, 3513–3570, 2006

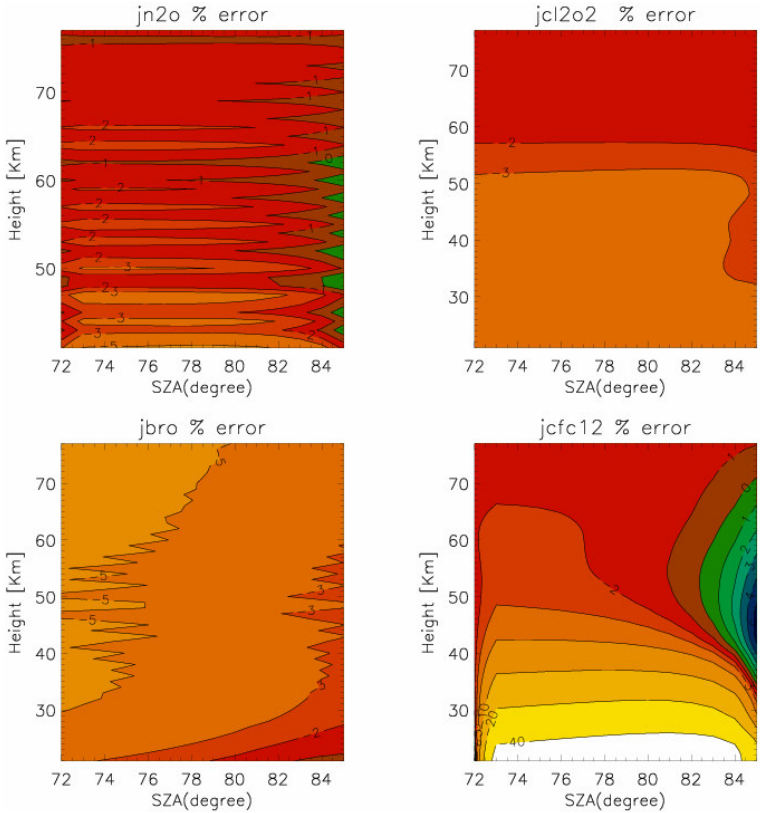

Fig. 5. The variation in the errors associated with the J values calculated using the band approach, with respect to the incident θ. Plots are shown for selected cases taken from the stratospheric subset of species (see Table 4) for a clear-sky scenario using the original band settings. The total ozone column was scaled to 300 DU and a ground albedo =5%.

ACPD
6, 3513–3570, 2006

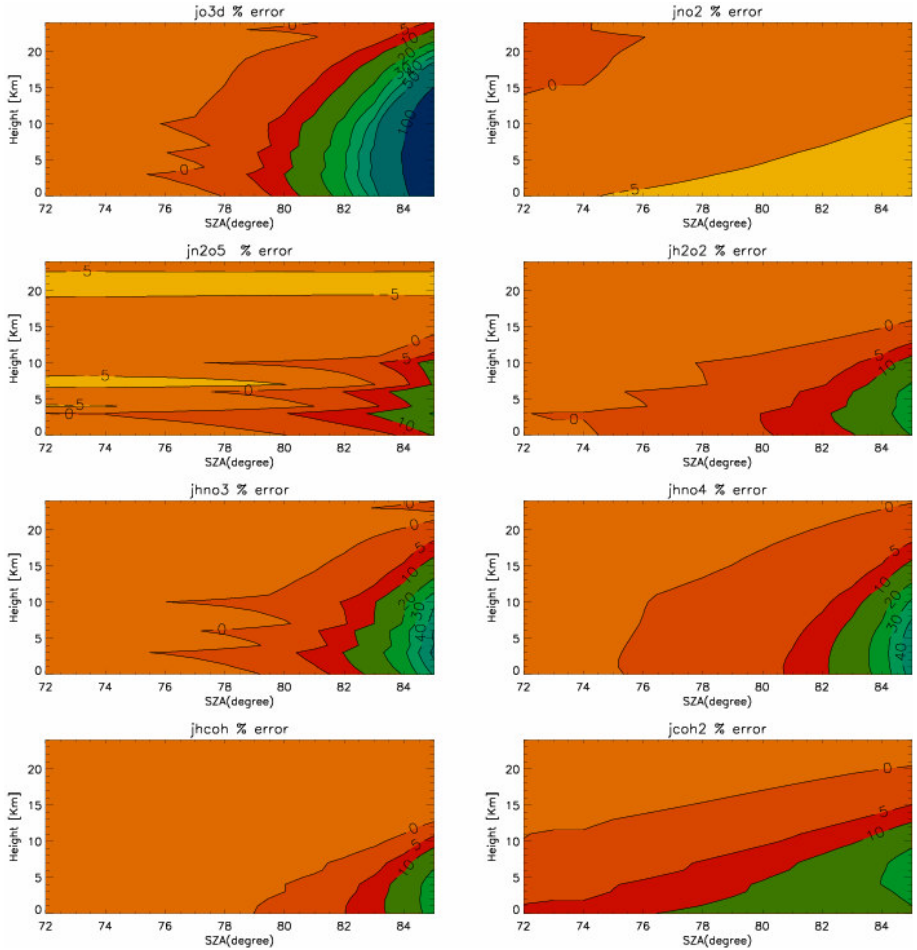

Fig. 6. The variation in the errors associated with the J values, with respect to incident θ, calculated for the tropospheric subset of species. Conditions are identical to those described for Fig. 5.

ACPD
6, 3513–3570, 2006

EGU

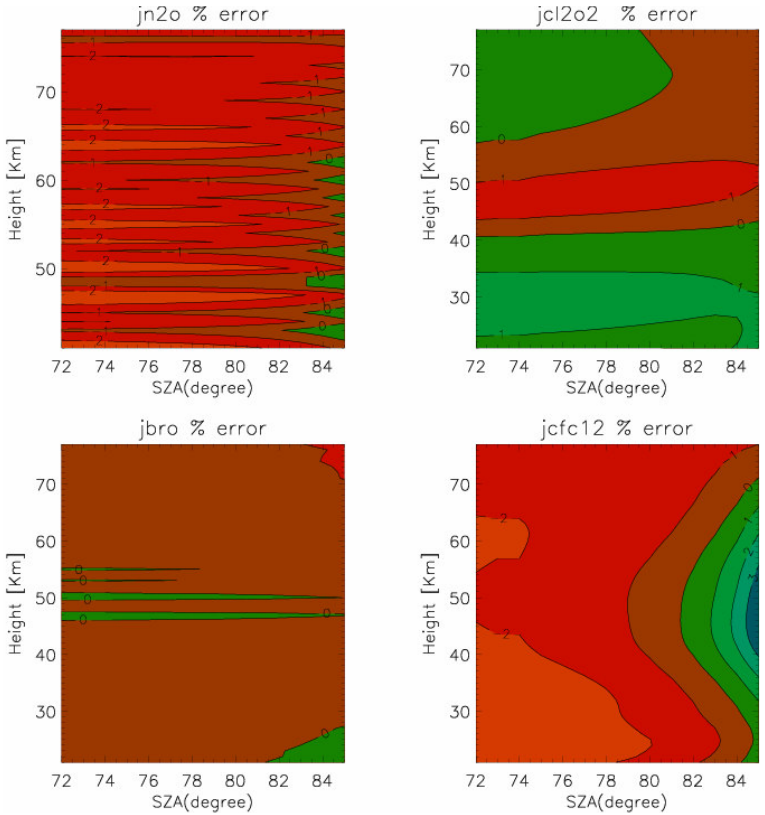

Fig. 7. The corresponding variation in the errors associated with the J values shown in Fig. 5 as a result of using the modified band approach in conjunction with grid A, with respect to the incident θ. Identical contouring is used to aid the comparison. The total ozone column was scaled to 300 DU and a ground albedo =5%.

ACPD
6, 3513–3570, 2006

EGU

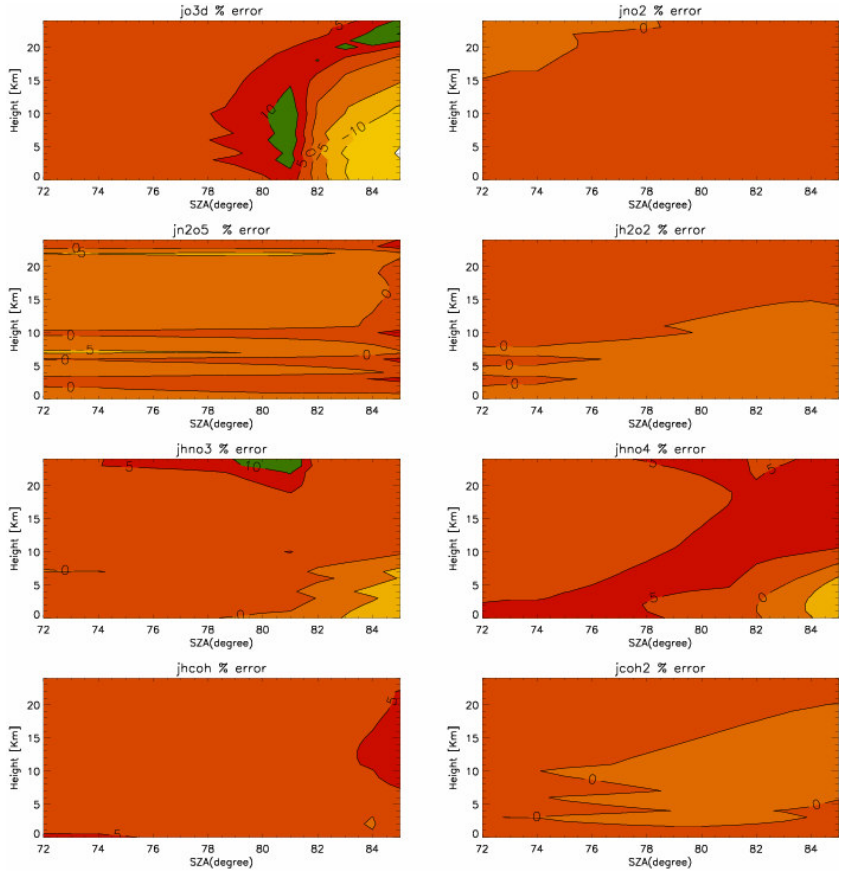

Fig. 8. The variation in the errors associated with the J values for the tropospheric subset of species with respect to the incident θ, as calculated using the modified band approach in conjunction with grid A. Conditions are identical to those described for Fig. 6 and identical contouring used to aid comparison.

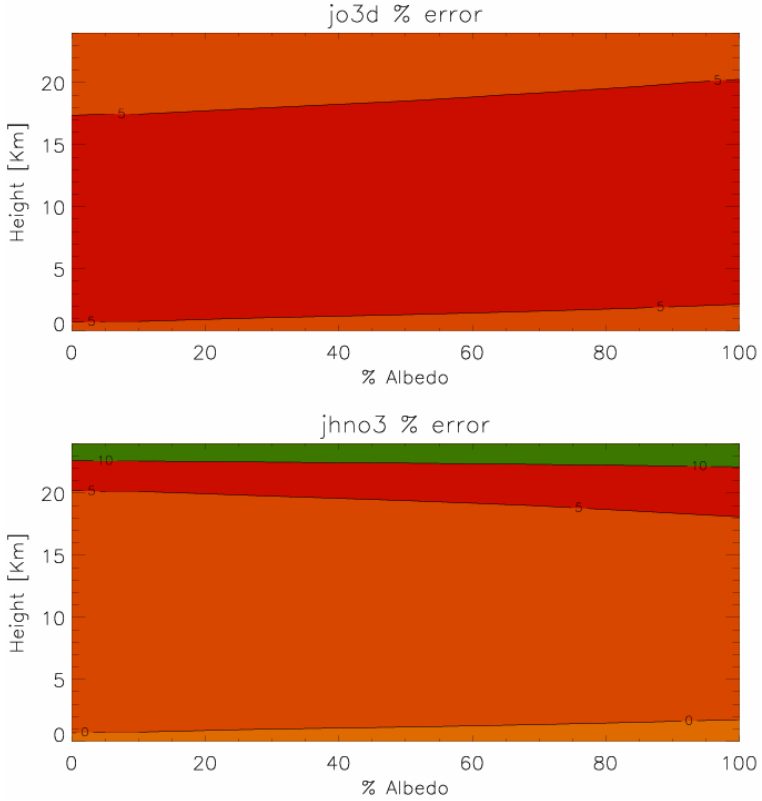

Fig. 9. The variation in the errors associated with the J values with respect to ground albedo for **(a)** O_3 and **(b)** HNO_3. A fixed θ=80° is applied under clear-sky conditions using grid A. The total ozone column was scaled to 300 DU.

ACPD
6, 3513–3570, 2006

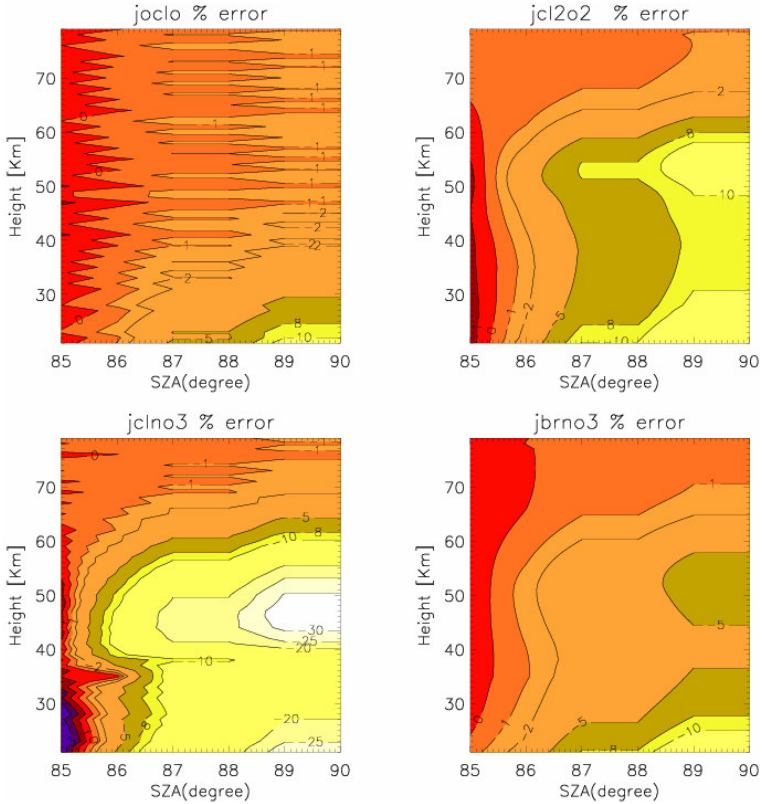

Fig. 10. The variation in the errors associated with the J values with respect to the incident θ as calculated for **(a)** OClO **(b)** Cl_2O_2 **(c)** $ClNO_3$ and **(d)** $BrNO_3$ for a clear-sky scenario using grid B. A threshold is applied to the scaling ratios (δ_i) used for the modified band approach which neglects the contribution made by certain bands once the direct flux falls below a prescribed value. The total ozone column was scaled to 300 DU.

ACPD
6, 3513–3570, 2006

EGU

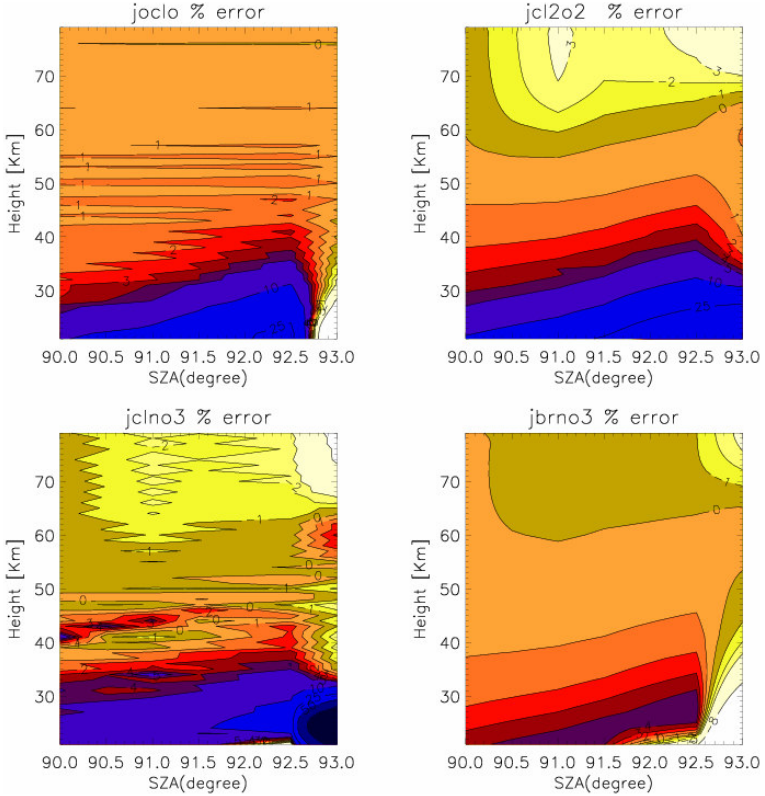

Fig. 11. The variation in the errors associated with the J values, with respect to incident θ, calculated for **(a)** OClO, **(b)** Cl_2O_2, **(c)** $ClNO_3$ and **(d)** $BrNO_3$ for a clear-sky scenario using grid B. An identical limit to the scaling ratios is applied as for Fig. 8. The total ozone column was scaled to 300 DU.

ACPD
6, 3513–3570, 2006

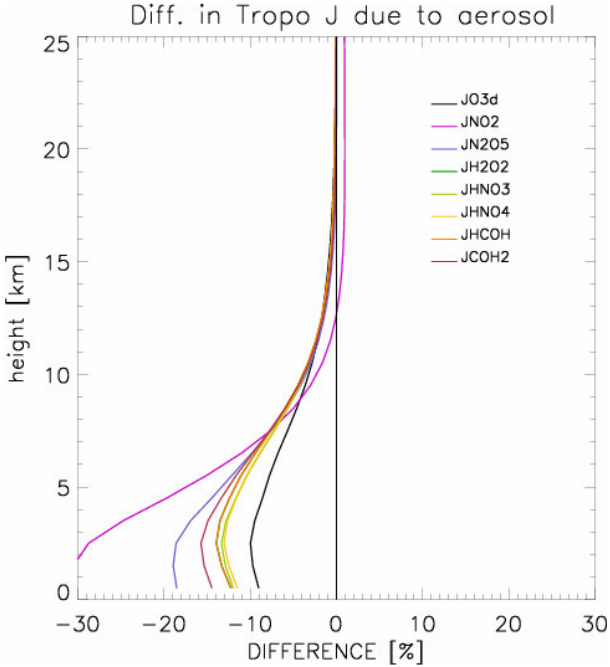

Fig. 12. The effect of aerosol particles on the J values for species contained in the tropospheric chemical subset at θ=80°. The optical density of the integrated aerosol column was scaled to 0.32 at 550 nm. Comparisons are made against J value profiles calculated using the modified band approach under clear-sky conditions. The ground albedo is 5% for all simulations.

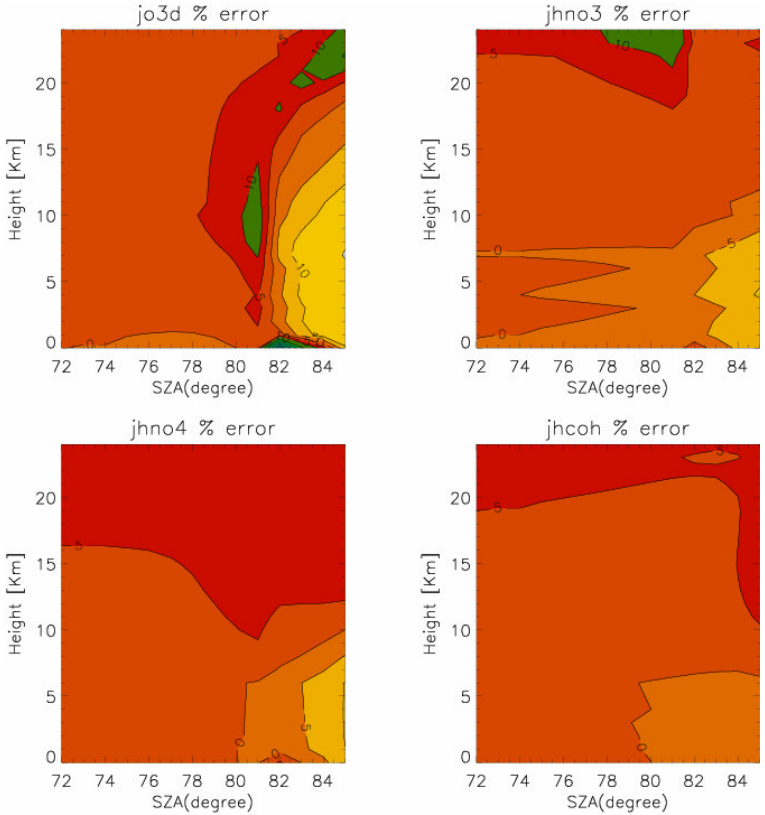

Fig. 13. The variation in the errors associated with **(a)** J_{O3d} **(b)** J_{HNO3} **(c)** J_{HNO4} and **(d)** J_{HCOH} with respect to the incident θ, in the presence of both cloud and aerosol calculated using the modified band approach grid A. The contouring used is identical to both Figs. 4 and 6 to aid comparison. All other conditions are identical to those used in Fig. 8.

ACPD
6, 3513–3570, 2006

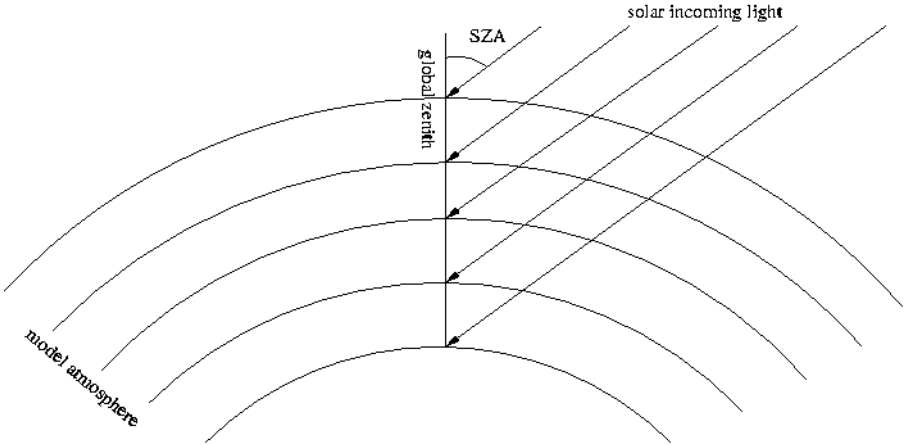

Fig. A1. Spherical geometry used for the pseudo spherical two-stream method. The solar radiation is calculated at the global zenith along its spherical light path through the atmosphere and then it is used as the source of solar light in a plane parallel atmosphere.

ACPD
6, 3513–3570, 2006

EGU

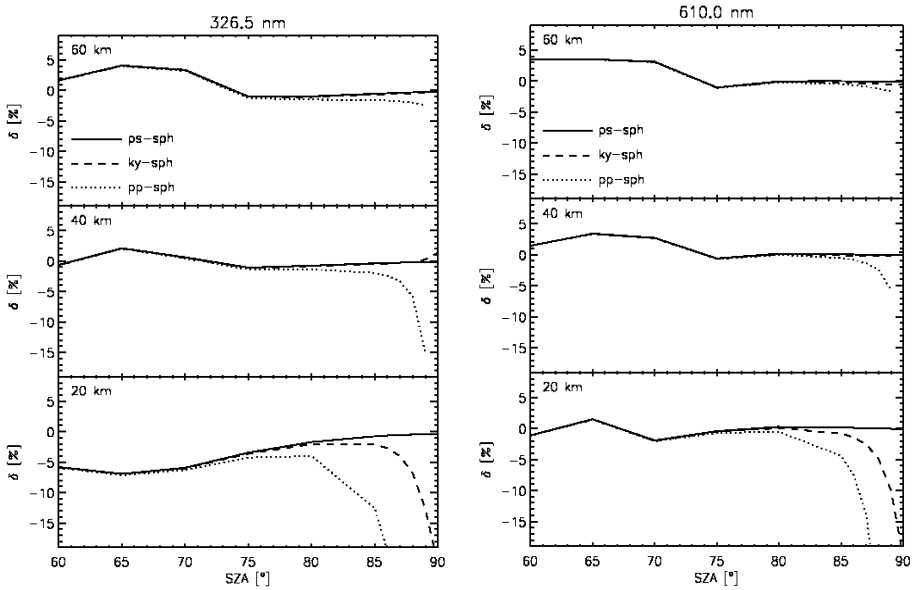

Fig. A2. Percentage differences (δ) in the actinic flux (F_{act}) calculated with different model versions of PIFM versus a full spherical radiative transfer model as a function of the solar zenith angle (SZA). Differences in F_{act} are shown for comparisons between the plane parallel PIFM version (pp), the version using the Kasten and Young correction for spherical air mass factors (ky) and the pseudo-spherical extension of PIFM (ps) versus the reference model (sph) at 20, 40 and 60 km altitude. The left panel shows differences for λ=326.5 nm and the right panel for λ=610.0 nm, which are pertinent to scaling wavelengths chosen for grid A (see Table 2). The model atmosphere is adopted from the US standard atmosphere 1976, albedo =0% and the total ozone column scaled to 300 DU.

ACPD
6, 3513–3570, 2006

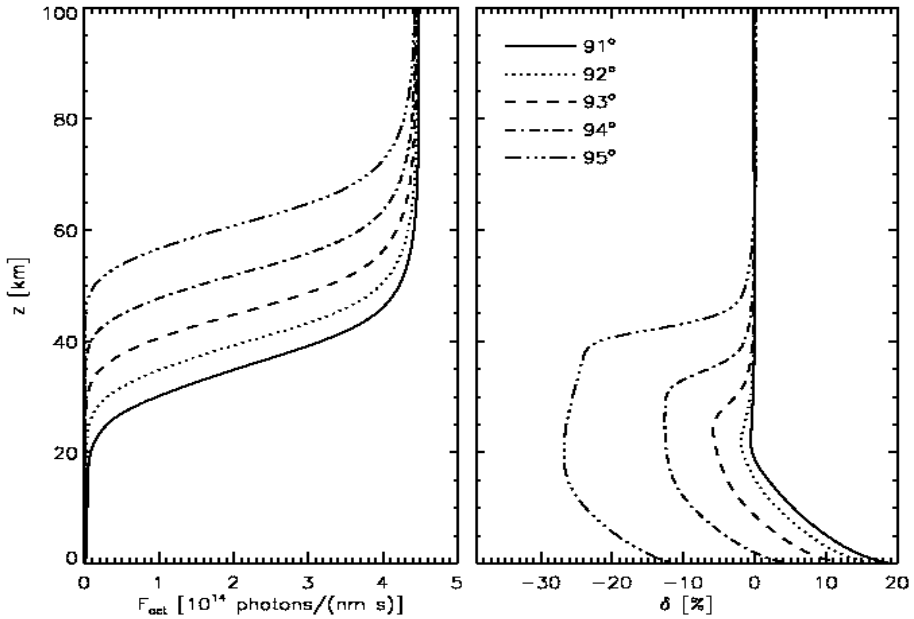

Fig. A3. The F_{act} at 326.5 nm as a function of altitude for θ=91–95 (left panel) and the associated error between the pseudo spherical PIFM model and the spherical reference model (right panel). The model atmosphere is the same as in Fig. A2.

ACPD
6, 3513–3570, 2006

EGU

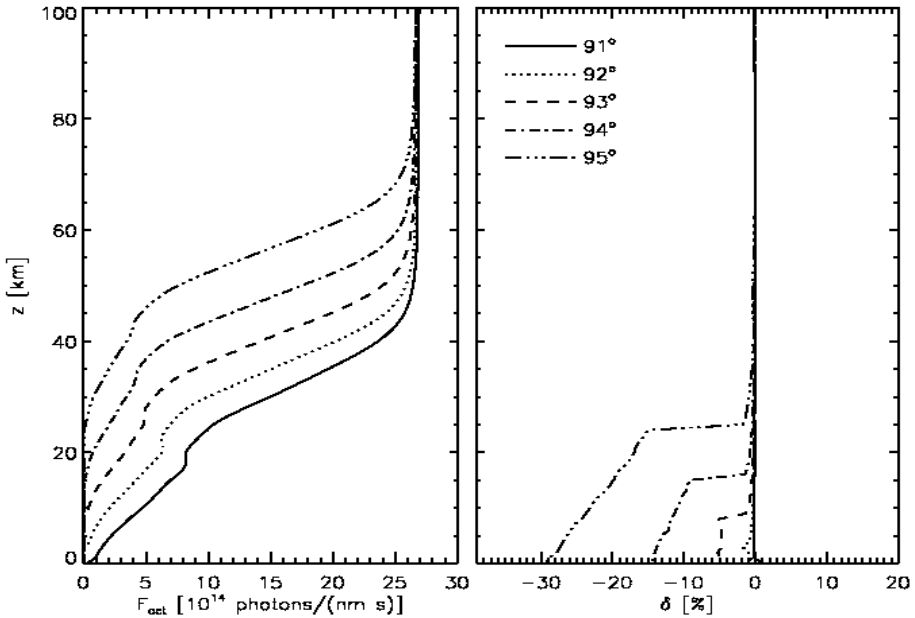

Fig. A4. Same as Fig. A3 but for 610.0 nm.

ACPD
6, 3513–3570, 2006

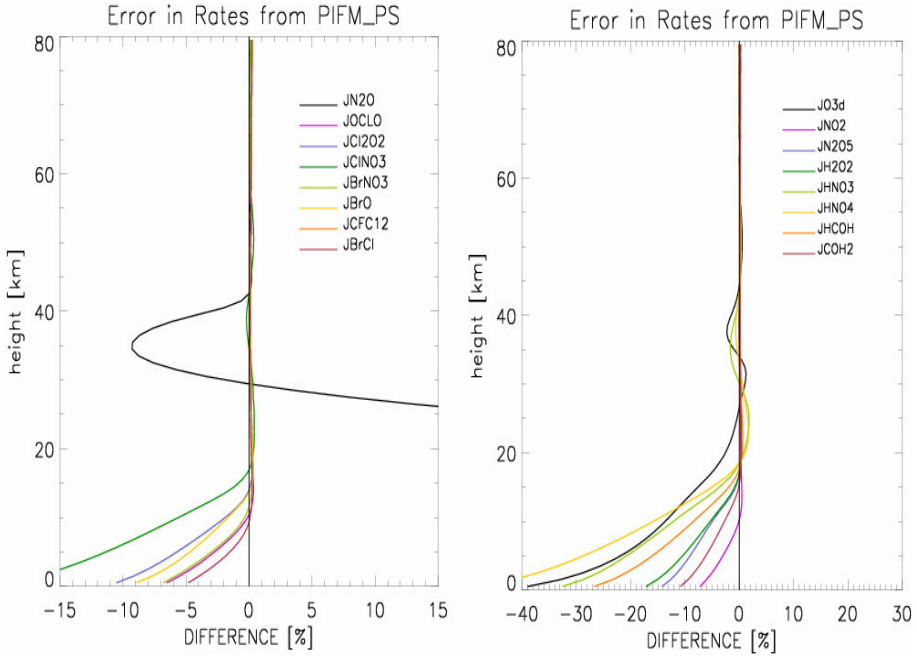

Fig. B1. Percentage errors associated with the J value profiles calculated using the PIFM-PS model as compared with reference model A at θ=90˚. For details regarding how the error was calculated the reader is referred to the text. Results are presented for **(a)** the stratospheric and **(b)** tropospheric chemical subsets, respectively. The model atmosphere is adopted from the US standard atmosphere 1976, albedo =0% and the total ozone column scaled to 300 DU.

ACPD
6, 3513–3570, 2006

EGU

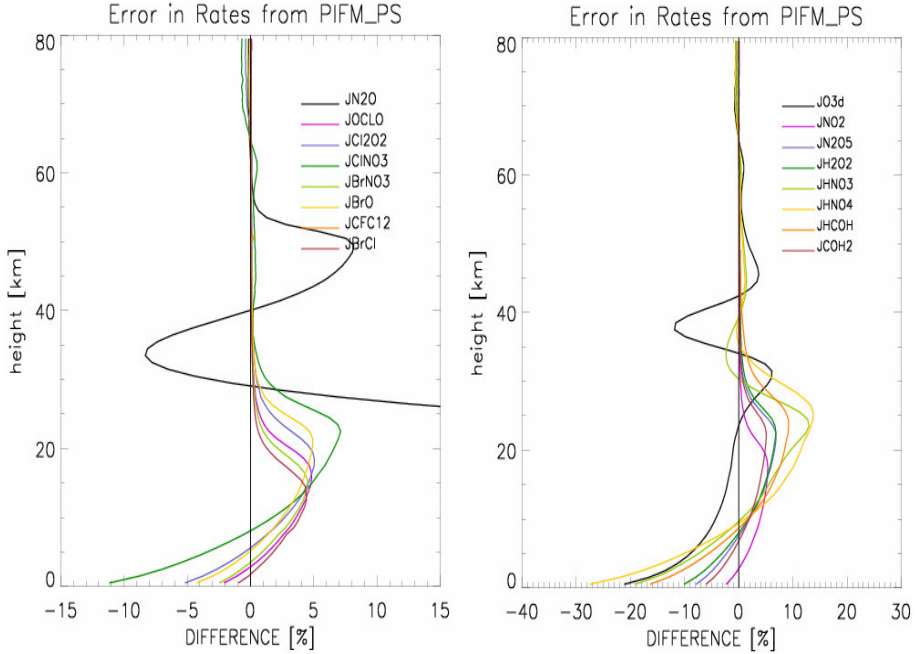

Fig. B2. As for Fig. B1 except the θ=93°.

ACPD
6, 3513–3570, 2006